MULTIPHASE FLOW AND CONSOLIDATION TESTING - ASHLAND/NORTHERN STATES POWER LAKEFRONT SUPERFUND SITE

Prepared for

Northern States Power Company - WI
1414 West Hamilton Avenue
Eau Claire, WI 54701

October, 2007

URS

6737 W. Washington Street, Suite 2265
Milwaukee, WI 53214
25688375

Executive Summary

This report presents the results of the Multiphase Flow and Consolidation Testing, one of several treatability studies recommended in the Candidate Technologies and Testing Needs Technical Memorandum [Treatability Studies Memorandum (Task 6 of the SOW): URS 2007a] that was originally submitted to USEPA on September 22, 2006 and approved on February 21, 2007. This test is a type of triaxial test setup known as a Seepage Induced Consolidation (SIC) test. The purpose of this testing is to provide data to be used for evaluating the technical implementability of capping and disposal technologies. The SIC setup was especially designed for very soft sediments to determine multiphase flow and consolidation properties of the sediments at low and medium high stress levels.

As explained in the introduction to the report, the SIC test works by subjecting a test sample to a constant downward flow rate and measuring the hydraulic pressure differential over the sample. As the stress is applied in this way, the pore fluid is expelled and consolidation occurs resulting in permeability changes within the sediment. These changes can be used to determine the:

1) Compressibility of the sediment;
2) Permeability of the sediment for gas (bubbles), water and non aqueous phase liquids (NAPL);
3) Threshold flow rate necessary to mobilize NAPL;
4) Threshold for air entry into the interstitial spaces which can then be used to evaluate the probability for gas bubble growth (ebullition); and
5) Amount of fluid released upon consolidation.

These characteristics can then be used as inputs to a model (the DELCON model) to predict the behavior of gas, fluid and NAPL in the underlying sediment during capping and during the period that underlying sediments are being consolidated by the cap. The cap can either be one that is applied subaqueously to in-place sediments or a cap applied to sediments after they have been deposited in a confined disposal facility (CDF).

The sediments used for this testing were collected by coring from a representative area of the Site known to be contaminated with polycyclic aromatic hydrocarbons (PAHs), volatile organic carbons (VOCs) and NAPL.

The SIC test was conducted using water, air (nitrogen) and NAPL (diesel fuel) as boundary conditions. Water, air and diesel fuel were forced through the sediment sample in separate tests and various measurements such as pressure, displacement and temperature were made.

A numerical model (DELCON) then was used to simulate the behavior of the sediments under a hypothetical subaqueous or CDF cap. In addition to the data developed in the SIC test supplemental data on the characteristics of Site sediment were used to "populate" the model. Characteristics of Site geology, bathymetry and stratigraphy also were incorporated into the model. Lastly, deposition rates of contaminated material and capping material for various

remedial alternatives as well as the properties of sand that will be used as cap material grain (particle) size distribution, minimum and maximum porosity, etc., were provided.

The DELCON model was used to simulate sediment behavior under two remedial alternatives: dredging and disposal into a CDF (SED 2) and placement of a subaqueous cap (SED 3). Results of the DELCON model indicated:

1) Under the CDF remedial scenario there would be relatively rapid consolidation of the wood layer under the CDF.
2) Only a small amount of consolidation in the Miller Creek clay layer under the wood layer will occur, but that will take place relatively rapidly (within the first five years).
3) Ebullition (gas release) in the underlying wood layer during the consolidation period is possible, however, conditions would no longer favor gas releases after the relatively rapid consolidation of the wood layer and the dredged slurry layer that would take place during the slurry deposition and cap placement time, say 180 days.
4) There would be no NAPL displacement expected from filling the CDF and subsequent consolidation since the predicted pore water discharges through the top layer of the dredged sediment are much smaller than are needed to mobilize NAPL.
5) Settlement consolidation after mechanical dredging under the CDF scenario was predicted to be almost the same as for the hydraulic dredging scenario because of the rapid consolidation of the wood layer beneath the CDF. Assuming the same depth CDF cap, settlement of the mechanically dredged material would be approximately 0.2 ft more than for settlement after hydraulic dredging.
6) Simulation of remedial scenario that includes dredging approximately 4 feet and then placement of a subaqueous cap, indicated that there would be virtually no consolidation of the native sediment given that the level cap re-establishes original bathymetry. Under this remedial scenario the discharges of pore water during capping are not sufficient to mobilize NAPL, nor should the capping result in gas releases substantially greater than what may presently occur.

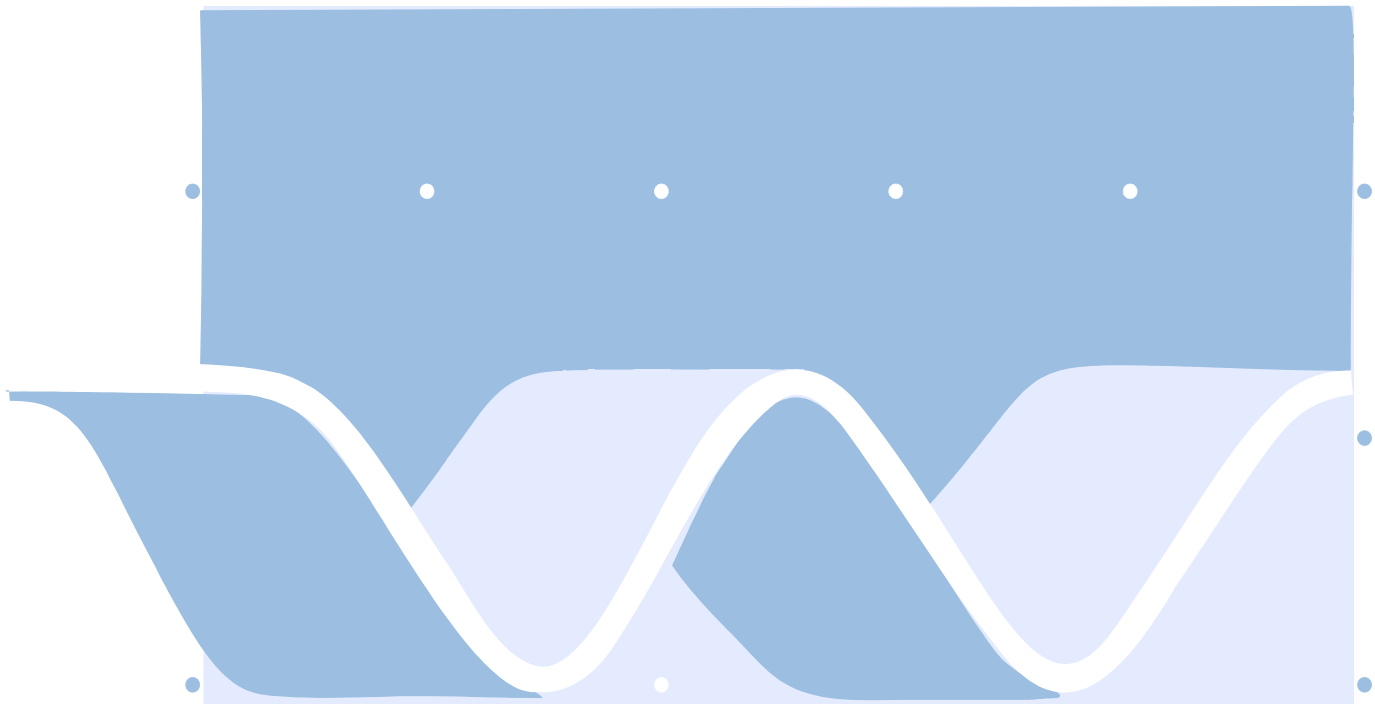

Multiphase Flow and Consolidation Testing: Ashland/Northern States Power Lakefront Superfund Site

Ashland, Wisconsin

Draft Report

October, 2007

Z4336

Prepared for:

URS Corporation

Prepared for:

URS Corporation

Walther van Kesteren

Draft Report

October, 2007

Contents

LIST OF ACRONYMS AND ABBREVIATIONS

CAD	Confined Aquatic Disposal Cell
CDF	Confined Disposal Facility
CF	Copper Falls Formation
CL	CLay deposit (Miller Creek Formation)
DELCON	DELft CONsolidation software for finite strain consolidation
FID	Flame Ionization Detector
GC	Gas Chromatograph
NAPL	Non Aqueous Phase Liquid
PAH	Polycyclic Aromatic Hydrocarbons
OM	Organic Matter
SIC	Seepage Induced Consolidation test
TOC	Total Organic Carbon
SD	SanD beach deposit (Miller Creek Formation)
SI	SIlt deposit (Miller Creek Formation)
VOC	Volatile Organic Compounds
WD	contaminated Wood Layer

LIST OF SYMBOLS AND UNITS

symbol	name	unit
A	activity	[-]
C_0, C_1	creep coefficients	[-]
c_v	vertical consolidation coefficient	[m^2/s]
c_u, c_{ur} [$Pa=N/m^2$]	undrained shear strength (remoulded)	
D_p ^6m]	pore diameter	[$\mu m=10^-$
e	void ratio	[-]
Fo	Fourier number	[-]
g	gravity acceleration	[m^2/s]
H	layer thickness	[m]
k	permeability	[m/s]
k^i_{NAPL}, k^i_w	intrinsic permeability NAPL and water phase	[m^2]
k_1, k_2	coefficents decay organic matter	[-]
LL	liquid limit	[% wt]
m_v	vertical compressibility	[m^2/N]
p_g	gas pressure inside bubble	[Pa]
p_{ae}	air entry suction pressure	[Pa]
PL	plastic limit	[% wt]

PI	plasticity index (=LL-PL)	[% wt]
S_v	specific surface area	[m^2/m^3]
t	time	[s, min, yr]
u_{cap}	capillary pressure	[Pa]
T	temperature	[^oC]
ε	vertical strain	[-]
η	dynamic viscosity	[Pas]
ν	kinematic viscosity	[m^2/s]
ρ	density	[kg/m^3]
σ	surface tension	[N/m]
σ'	effective stress	[Pa]
ξ_I	solid fraction by weight	[-]
ξ^{OM}	organic content by weight	[-]

1. Introduction

As part of the treatability testing for the remedial investigation and feasibility study at the Ashland/Northern States Power Lakefront site in Ashland county, Wisconsin (see Fig.1), URS requested WL|Delft Hydraulics perform combined multiphase flow and consolidation experiments in the triaxial test set-up known as the Seepage Induced Consolidation (SIC) test. The combined multiphase flow and consolidation parameters are used to model impacts of capping of in-place sediments, i.e. subaqueous capping, or for dredged material disposal in a confined aquatic disposal cell (CAD), or in a confined disposal facility (CDF) when sediments are dredged and placed in these disposal facilities. The results of this testing will be used by URS to evaluate the implementability of capping, dredging and disposal technologies. For this evaluation, quantification of the behavior of gas, NAPL and fluid in the sediment beneath a cap or in a CDF is required. Therefore this report also includes simulations with the DELCON model, which predicts gas, NAPL and fluid behavior during deposition, consolidation and capping as function of time, depth and temperature.

Figure 1.1 Location Ashland site

2. Objective and Scope of Work

2.1 Objective

The objective of the experimental study is to determine multiphase flow and consolidation properties of contaminated sediment from the Ashland site (Site), and apply the results in simulations with the DELCON model for gas, NAPL and fluid behavior in the sediment beneath a cap or in a CDF. Data derived from this study will be used for evaluating the technical implementability of several remedial alternatives for sediments.

2.2 Scope of work

In the experimental study the multiphase flow and consolidation properties of Site sediments were determined with the SIC test. In this test consolidation can be realized in two ways:

- loading by a constant discharge through the sample, which results in consolidation only at the lower boundary
- loading by an external load, which results in consolidation over the full height of the sample)

The SIC test set-up, shown in Figure 2.1, was especially designed for very soft sediments to determine multiphase flow and consolidation properties at low and medium high stress levels. A constant flow rate through the sample downwards is precisely controlled by a syringe pump with the suction side connected to the lower drain system. In the drain system the hydraulic pressure is measured with a transducer with respect to the cell pressure. This pressure difference consolidates the sediment, which is measured with a displacement gauge. As the pore fluid is expelled, consolidation occurs and the permeability changes. By measuring the pressure difference for different flow rates the permeability and effective stress as function of void ratio can be determined.

When an external load is applied to consolidate the sample, the lower drain system is closed and the syringe pump is inactive. As a result, expelled pore water is drained through the top platen.

The multiphase flow characteristics of the NAPL/water pore system are dependent upon the threshold for NAPL flow and intrinsic permeability of water phase and NAPL phase in the pore system. These properties are determined by seepage tests at different discharge rates, where the boundary at the top platen is either water or NAPL. For the NAPL boundary diesel fuel is used in these SIC tests. When the diesel in the top platen chamber is not entering the sample the settlement of the top

platen equals the applied specific discharge and the sample consolidates. When diesel enters the sample the settlement will be less than the applied specific discharge and the difference is the amount of diesel in the sample. The total amount of diesel that went through the sample is measured together with the amount of diesel in the sample after the test. The threshold for NAPL flow is determined by its rheological properties in terms of apparent viscosity. Given the higher molecular weight (higher Cn) of the NAPL present in the sample than diesel, the apparent viscosity will be higher and therefore the measured threshold level can be regarded as a minimum.

Figure 2.1 Seepage Induced Consolidation test set-up

The SIC test has been used to:

1. measure the settlement characteristics (compressibility) of the sediment matrix;
2. measure the permeability of the sediment for gas, water and NAPL;
3. determine the threshold flow rate that is necessary to mobilize NAPL;
4. determine the threshold for air entry in the pore system, which is important for evaluating the potential for gas bubble growth (ebullition) in the sediment matrix;
5. measure the amount of fluid released upon consolidation.

Besides the SIC tests, supplemental analyses were performed for determining sediment properties that are necessary for the DELCON simulations. Some of these properties are also required as a reference to compare to the results of other treatability testing conducted on Ashland sediment, i.e., the cap flux testing.

In the associated numerical study, simulations were performed with the DELCON model, which can compute multiphase flow and consolidation of the contaminated sediments during deposition and after capping. The required input data for DELCON was obtained from the SIC tests and the supplemental testing. The

simulation was conducted for the local boundary conditions and lithographic structure.

The following tasks were defined:

Task 1 Seepage Induced Consolidation tests

The following 2 SIC tests were performed on the contaminated sediment:

- SIC test with water boundary; at the end of the test a gas boundary was applied in order to determine the "air entry value"; and
- SIC test with NAPL boundary (diesel fuel) in order to determine threshold flow rate to mobilize NAPL.

Diesel fuel is used as hydrophobic (non-wetting) fluid in the pore system and as solvent for the NAPL phases in the pore system.

The duration of each test depends on consolidation characteristics of the sediments

Task 2 Supplemental analyses

Supplemental analyses were conducted to measure additional sediment properties for DELCON simulations and as a reference. The following supplemental analyses were conducted on the contaminated sediment:

- Gas content (methane and carbon dioxide) and gas production rates (4 temperatures) (WL|Delft Hydraulics; see Fig.2.2);
- Water content (WL|Delft Hydraulics);
- Grain (particle) size distribution (GeoDelft);
- Atterberg limits (plasticity and liquid limit) (GeoDelft);
- Total organic carbon (TOC) (GeoDelft);
- Carbonate content (GeoDelft);
- TerrAtest on filtrate SIC test measuring PAHs, VOCs and mineral oil (Analytico); and
- NAPL content in sediment measuring PAHs and mineral oil (Analytico).

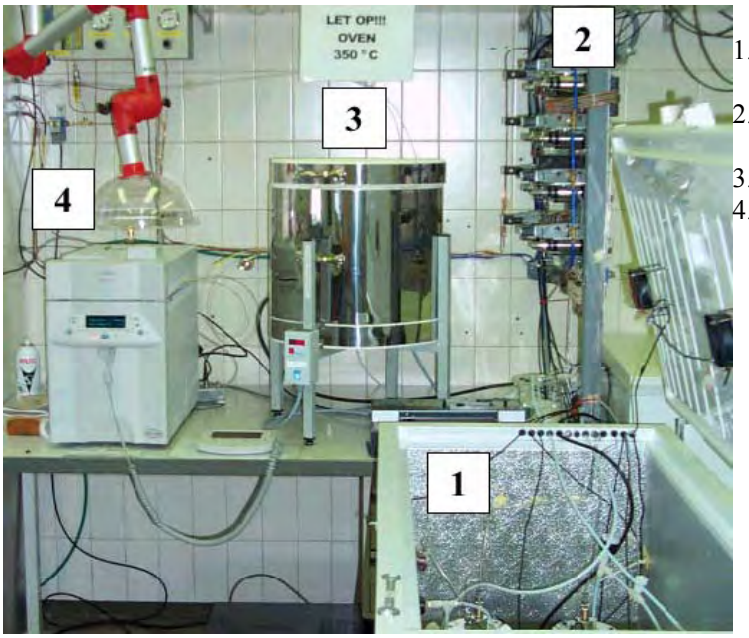

1. refrigerator with samples
2. switch and sampling loops
3. methanizer for CO_2
4. Gas Chromatograph

Figure 2.2 Gas generation test set-up at WL|Delft Hydraulics

Task 3 Data analysis

The analysis of the SIC tests assessed:

- settlement characteristics (compressibility) of the sediment matrix;
- permeability of the sediment for gas, water and NAPL;
- threshold flow rate that is necessary to mobilize NAPL; and
- amount of fluid released upon consolidation.

These results and the results from the supplemental analyses were used as input data for the DELCON model.

Task 4 DELCON simulations

DELCON simulations are performed for 2 alternatives:

1) Dredge sediment and place dredged slurry in a confined disposal facility (CDF) on site. The CDF will be capped with a sand cap of variable thickness (2, 3.5, 5.2 and 7 ft).
2) Dredge surface sediment (2-4 feet) and cap the whole dredged area with sand with variable thickness. (1, 2, 3, 4 or 5 ft).

It was assumed that the surcharge sediment has the same properties as the contaminated sediment, except for the contamination levels, and that the base sediment underlying the CDF is consolidated clay with properties measured by the cores collected during the field program.

For each alternative, varying cap layer thicknesses have been simulated. The simulation output consisted of a time series of sediment layer thickness, water content as function of depth, gas- NAPL- and water-fluxes through all sediment layers and gas ebullition fluxes.

For the simulations the following information was provided by URS:

- Local lithographic structure including aquifers (if any);
- Boundary conditions pore water pressures;
- Water level;
- Seasonal temperature variations;
- Deposition rates of contaminated material and capping material;
- Properties of sand that will be used as cap material (grain (particle) size distribution, minimum and maximum porosity); and
- Properties of base clay sediment layer (consolidation properties and water content as function of depth).

3. Seepage Induced Consolidation Tests

3.1 Sample preparation

Two sample cores from the Site were shipped to Delft and received on 12 March 2007. These two cores were taken in Area 2 (see Fig.3.1): Core sample 200 ft SE and core sample 150 ft W (the nomenclature for these samples is based upon the grid coordinates at the Site). Only the first core was used for testing. The 2nd core was back-up in case of test failures or sample losses. The upper half of the core volume was tested by GeoDelft for supplemental analyses (see Ch.4), the other half was used for SIC tests. Given the size of the brass sample ring in the SIC facility (height 30 mm, diameter 83 mm) the wood particles larger than 10 mm were separated by sieving. The composition of the original sample and sieved sample are provided in Table 3.1. In order to determine the water phase, wood phase, mineral phase and NAPL phase, subsamples were dried at different temperatures:

105 ^{o}C: evaporation of pore water and VOC's

450 ^{o}C: humus content without decomposing carbonates

1100 ^{o}C: burning all organic mater and decomposing carbonates: mineral solids

Carbonate content is determined on the residue after 450 ^{o}C.

The 36.8% coarse material (>10 mm) is not able to build up a skeleton[1] by its own in the original sediment and therefore the skeleton of the sediment is determined by the fraction smaller than 10 mm. The coarse fraction (>10 mm) is only occupying space in the original sediment and therefore will affect permeability and compressibility by its volume fraction. The results of the SIC tests can be corrected for this presence of the coarse material.

Table 3.1 Sample composition

	GeoDelft < 2.8 mm	**Delft Hydraulics < 10 mm**	**Delft Hydraulics > 10 mm**	**total Delft Hydraulics**
fraction by weight [%]		63.2	36.8	100
water content W [%]	385.4	401.5	251.2	337.7
solid content C [%]	20.6	19.6	28.5	23.1
mineral content [%]	44.3	32.8	16.1	25.2
organic content [%]	52.1	63.5	78.7	70.4
carbonate content	3.6	3.6	5.3	4.4

[1] The skeleton of solids in a sediment is defined as the solid matrix that is transferring stresses.

[%]				

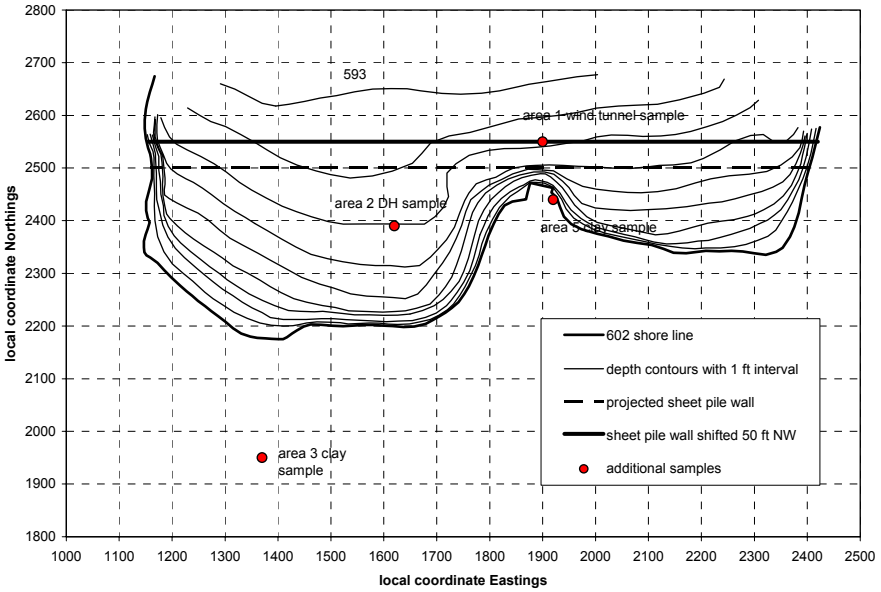

Figure 3.1 Sample locations in Ashland site

3.2 Test Set-up - Seepage Induced Consolidation

A schematic set-up of the SIC test is given in Fig.3.2. The main components are the flow controlled pump and the triaxial cell that contains the brass ring with sample and filter stones and filter paper on both sides. The drain system below the sample is connected with the pump. On top of the sample different boundary conditions can be applied. The top platen has a chamber in which different liquids can be placed or just used for the gas phase of the cell. The chamber can be loaded with an external load. The flow controlled pump generates a negative pressure in the drain system that forces pore fluid to flow downwards (seepage). Due to the hydraulic gradient the sample starts consolidating at the lower boundary of the sample.

The following 2 SIC tests were conducted on the contaminated sediment:

- SIC test with water boundary; at the end of the test a gas boundary is applied
- SIC test with NAPL boundary (diesel fuel)

Five tests were conducted (see Table 3.2); the first 2 of which were with water boundary and failed due to small wood fragments that got stuck in between the brass ring and

Table 3.2 SIC test program

Test number	boundary	before test			after test		
		W %	c_u Pa	$c_{u,r}$ Pa	W %	c_u Pa	$c_{u,r}$ Pa
SIC #1	water	425					
SIC #2	water	425					
SIC #3	water	425	196 169	39 39	256	39000	1800
SIC #4	diesel fuel	351			244		
SIC #5	air	301			224		

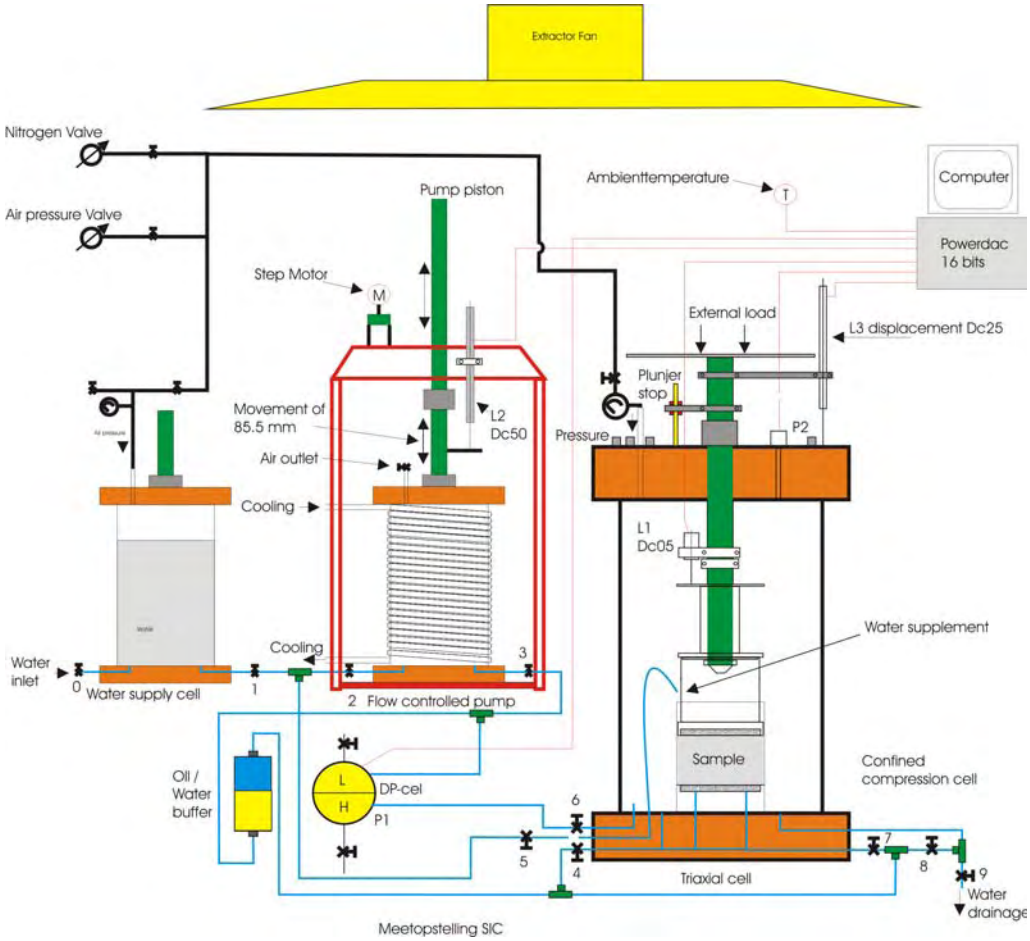

Figure 3.2 Test set-up Seepage Induced Consolidation

the top platen. The 3 following tests worked well. It was decided to do the gas boundary on a separate sample in order to be able to determine the "air entry value" at low effective stress. It is necessary that the capillary force is able to show displacement of the top plate before air enters the sample. Furthermore a separate test enables the measurement of water content and vane shear strength after the test

with the water boundary (SIC#3). The initial water content and water content after the tests are given in Table 3.2. Also the undrained peak and remoulded shear strength for SIC#3, are included (see Ch. 4.2).

All SIC tests were executed with the same sequence of loading steps as given Table 3.3. The first load of 363 Pa is the weight of the top platen. After consolidation, seepage suction with the piston pump was applied. This pump yields a controlled downward flux of pore water through the sample. Six different discharges were applied (see Table 3.3): 7.68, 15.72, 31.45, 47.27, 62.9 and 78.62 mm^3/s. The 2^{nd} discharge was applied first, in order to get the piston pump started. By measuring the pore pressure in the drain below the sample the permeability was determined as function of the discharge.

Additional loading was applied by external weights on the sample. The drain below the sample was closed during the loading in order to measure the change in pore water pressure during consolidation. In total 5 external loads were applied: 4092, 11551, 22740, 33929 and 70191 Pa. After consolidation of each loading step a seepage suction sequence of six discharges was applied. The last stage of the test is unloading the external loads.

Table 3.3 Loading steps in SIC-test

loading step	**load [Pa]**	**discharge [mm^3/s]**
top platen	363	
seepage		15.72, 7.68, 31.45, 47.27, 62.9, 78.62
external load	4092	
seepage		15.72, 7.68, 31.45, 47.27, 62.9, 78.62
external load	11551	
seepage		15.72, 7.68, 31.45, 47.27, 62.9, 78.62
external load	22740	
seepage		15.72, 7.68, 31.45, 47.27, 62.9, 78.62
external load	33929	
seepage		15.72, 7.68, 31.45, 47.27, 62.9, 78.62
external load	70191	
seepage		15.72, 7.68, 31.45, 47.27, 62.9, 78.62
unloading		

3.3 Test results Seepage Induced Consolidation

3.3.1 Test SIC#3

During the test the following data were collected:

- pore water pressure in the drain below the sample with respect to cell pressure;
- vertical displacement of the top platen inside cell;
- vertical displacement of top platen during external loading outside cell;

- vertical displacement of piston pump;
- absolute pressure outside cell;
- pressure inside cell; and
- temperature.

A typical result of an external loading step is shown in Fig. 3.3 for SIC#3 (70191 Pa), where the vertical displacement or settlement and pore water pressure is plotted as function of time. The consolidation phase is relatively short and in most cases less than 100 minutes. The consolidation phase corresponds to the change in pore water pressure. After 10 minutes the pore water pressure is stabilizing. However the vertical displacement is continuing (creep) and shows on logarithm time scale a linear relationship.

This creep can be modeled by:

$$\varepsilon = C_0 + C_1 \ln(t) \quad (3.1)$$

in which ε is the vertical strain, t time in minutes, C_0 and C_1 creep coefficients.

The creep coefficients were determined from the linear fit on logarithm time scale. This was only done for SIC#3.

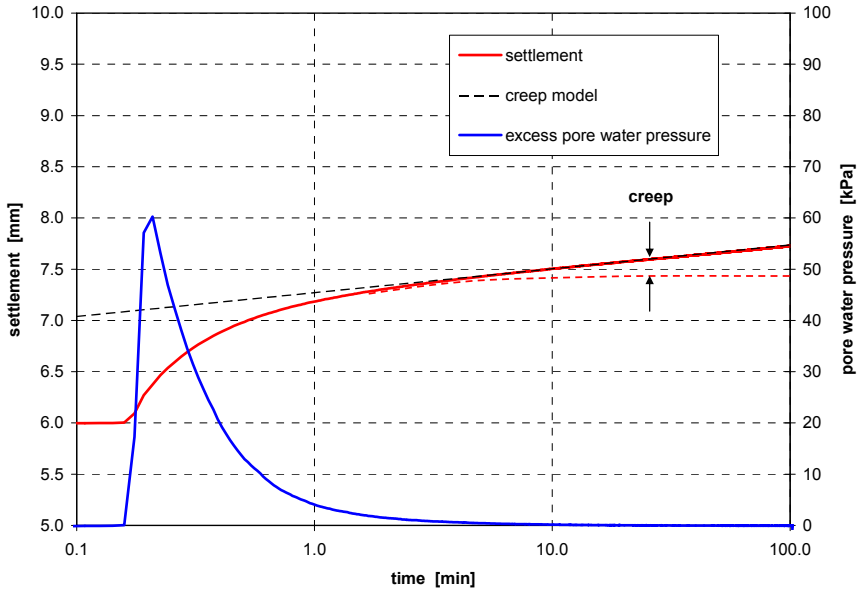

Figure 3.3 External loading step to 70191 Pa SIC#3

A typical result for the seepage loading phase is given in Fig.3.4, where the vertical displacement and water pressure in the drain is plotted as function of time. The water pressure response is within several seconds, resulting in a step wise pore water pressure change for the six different discharges. At higher discharges the step has a

linear increase in suction pressure, which is more as discharge increases. This is caused by the decrease in water level on top of the sample. The vertical displacement is relatively small during the seepage steps and is the example about 0.02 mm. In Fig.3.5 the measured pore water pressures are plotted as function of discharge. In most cases the data points show a linear relationship, from which the permeability can be determined. In the multiphase SIC tests #4 and #5 the relationship is not always linear as will be discussed in section 3.3.2 and 3.3.3.

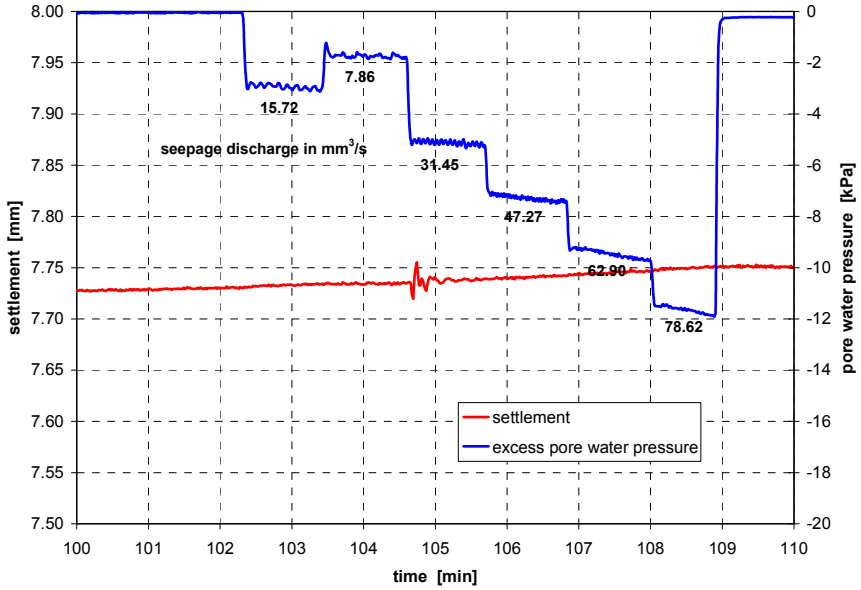

Figure 3.4 Seepage loading step at 70191 Pa SIC#3

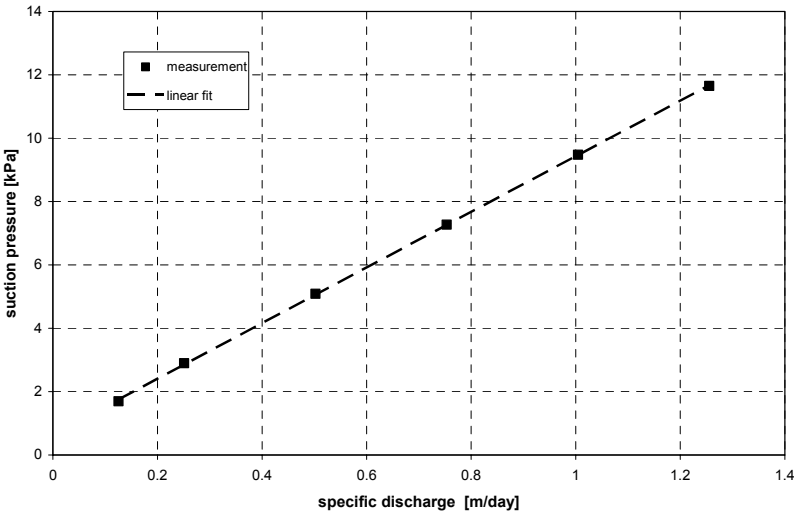

Figure 3.5 Determining permeability from seepage loading step at 70191 Pa SIC#3

From the consolidation at different vertical effective stresses the relationship between effective stress and void ratio is obtained. This is shown in Fig.3.6. The data are fitted with the power law model that is used for the DELCON computations:

$$e = A(\sigma' + Z)^B \qquad (3.2)$$

in which e is void ratio, σ' is vertical effective stress [kPa], A and B coefficients of the power law model and Z is coupled to the void ratio at zero effective stress.

The coefficients are given in Table 3.4. In Fig.3.6 the measured peak strength is also plotted (see Table 3.2).

The permeability as function of void ratio is shown in Fig.3.7 and shows also a power law relationship:

$$k = C\,e^D \qquad (3.3)$$

in which e is void ratio, k is permeability [m/s], C and D coefficients of the power law model.

The coefficients are given in Table 3.4.

From eq.(3.2) and eq.(3.3) the consolidation coefficient can be determined:

$$c_v = \frac{k}{\gamma_w m_v} \; ; \; m_v = -\frac{\mathrm{d}e}{\mathrm{d}\sigma'}\frac{1}{1+e} \quad \Rightarrow c_v = \frac{C}{\gamma_w B} A^{-1/B} e^{D-1+1/B}(1+e) \qquad (3.4)$$

in which c_v is consolidation coefficient [m^2/s], γ_w is specific weight water [kN], m_v compressibility [m^2/N].

The consolidation coefficient is plotted in Fig.3.6 and is about 2.4 10^{-5} m^2/s in the test range.

Table 3.4 Coefficients SIC#3

A	***B***	***Z***	***C***	***D***
5	-0.128	5.71623	2.2610E-11	8.35080

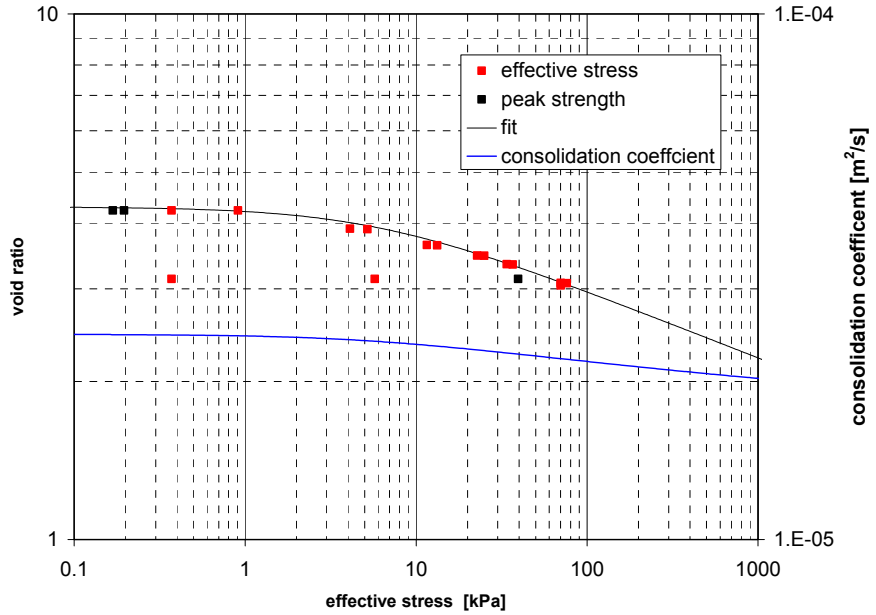

Figure 3.6 Effective stress and peak strength as function of void ratio SIC#3

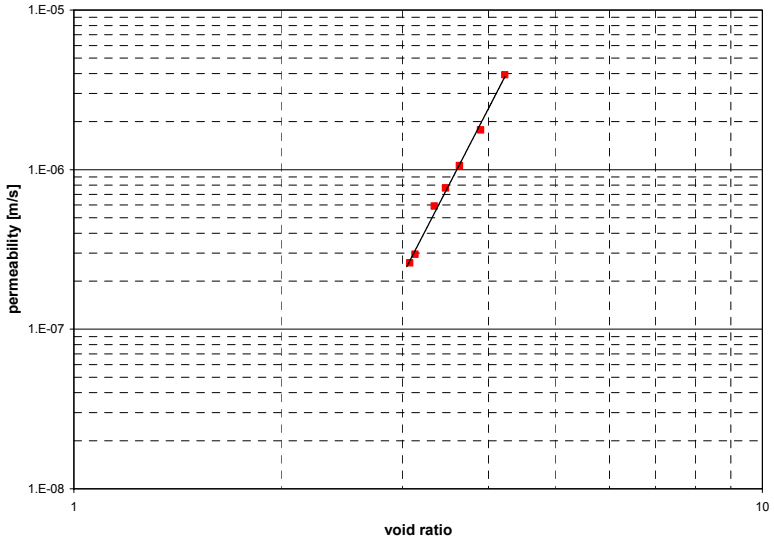

Figure 3.7 Permeability as function of void ratio SIC#3

The typical time scale for consolidation is obtained from the Fourier number defined by:

$$Fo = \frac{c_v t}{H^2} \tag{3.5}$$

in which t the time [s] and H the layer thickness [m] with drainage on both sides.

The layer thickness in the SIC test is 0.03 m, but with only drainage on the upper boundary. Therefore H is 0.06 m and results in a time scale for consolidation of 2.5 min. This corresponds well with the time scale observed in Fig.3.3.

The creep coefficients are determined for the different effective stress loadings and are shown in Fig.3.8. The fits are used in the DELCON computation for the long term settlements and are given by:

$$C_0 = 6.0067 \cdot 10^{-2} \ln(\sigma') - 0.43524$$
$$C_1 = 9.1738 \cdot 10^{-4} \ln(\sigma') - 6.8865 \cdot 10^{-3} \qquad (3.6)$$

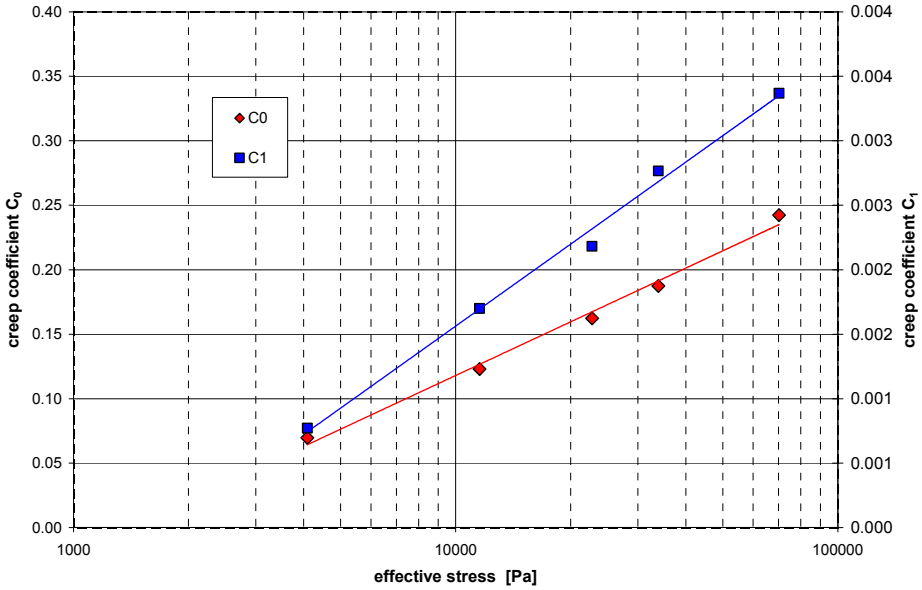

Figure 3.8 Creep coefficients as function of effective stress SIC#3

3.3.2 Test SIC#4

This test is performed with a diesel boundary on top of the sample. The diesel fuel has a density of 824 kg/m^3 and dynamic viscosity of 4.43 mPas (at 20 ^{o}C). During the consolidation by the vertical loading the diesel boundary will be pushed upward in the sample and will go downwards during the seepage loading phases. The relationship between effective stress and void ratio is given in Fig.3.9 and is similar to SIC#3 which fit is also shown. The coefficients for SIC#4 are listed in Table 3.5.

The permeability shows a different behavior as function of the specific discharge due to the entrainment of diesel in the sample. This is depicted in Fig.3.10 where the permeability is given as function of specific discharge for different consolidation stresses. At low effective stresses (black squares) the relationship is linear, but at 4092 Pa effective stress an increase in the slope is observed above a discharge of 0.75 m/day. The increase in suction pressure is related to the entrainment of diesel

fuel in which surface tension between diesel, water and solid are important. At higher effective stresses the relationship is reversed with a lower gradient above 0.75 m/day than below 0.75 m/day specific discharge. In Fig.3.11 the gradients above 0.75 m/day are shown with blue squares and indicate an increase in permeability. This increase is related to the contribution of pores filled with the NAPL phase of the initial sediment. The threshold flow rate for mobilizing the NAPL phase is 0.75 m/day.

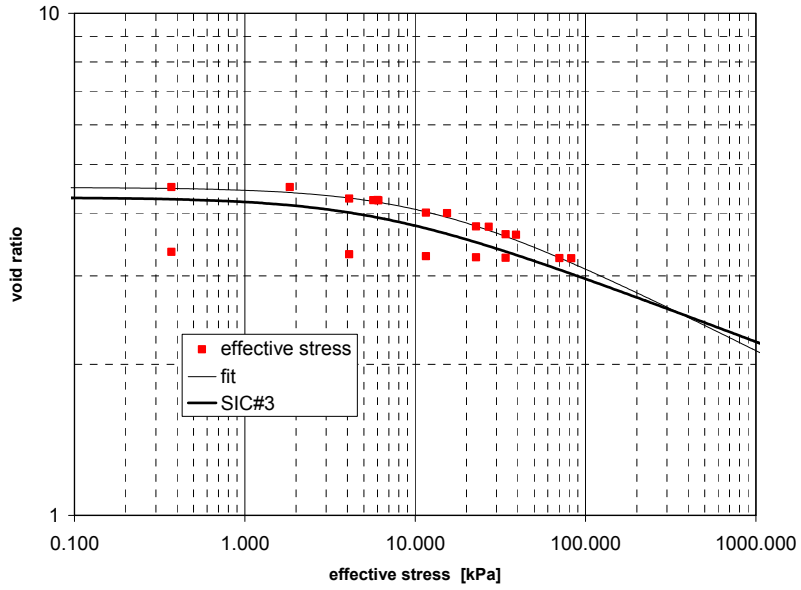

Figure 3.9 Effective stress as function of void ratio SIC#4

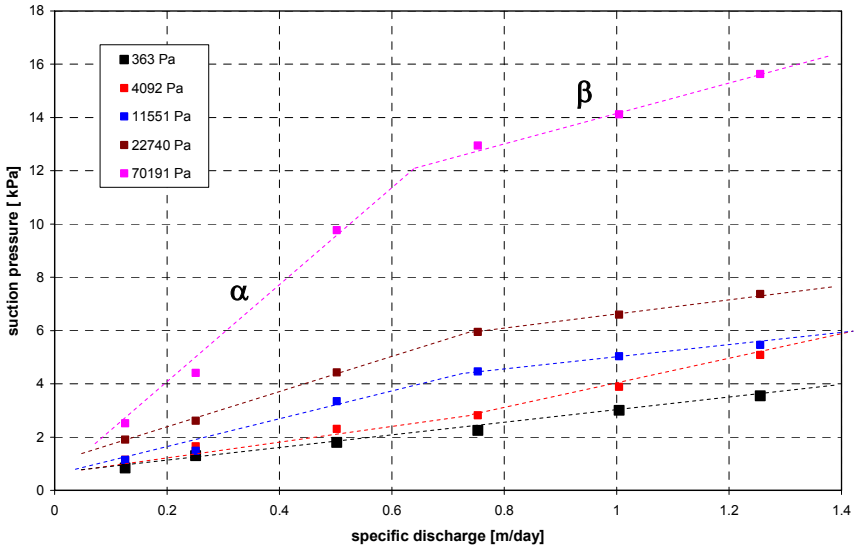

Figure 3.10 Permeability as function of specific discharge SIC#4

From the ratio in gradient before (α) and after the threshold flow rate (β) the intrinsic permeability of the water phase and NAPL phase can be determined (see. Marle, 1981):

$$\frac{\eta_w}{k_w^i}\frac{k_{NAPL}^i}{\eta_{NAPL}} = \frac{\alpha}{\beta} - 1 \quad ; \alpha = \frac{\eta_w}{k_w^i} \quad ; \quad \frac{1}{\beta} = \frac{1}{\alpha} + \frac{k_{NAPL}^i}{\eta_{NAPL}} \tag{3.7}$$

in which η_w is dynamic viscosity water [Pas], η_{NAPL} is dynamic viscosity NAPL [Pas], k_w^i intrinsic permeability water phase [m^2] and k_{NAPL}^i intrinsic permeability NAPL phase [m^2].

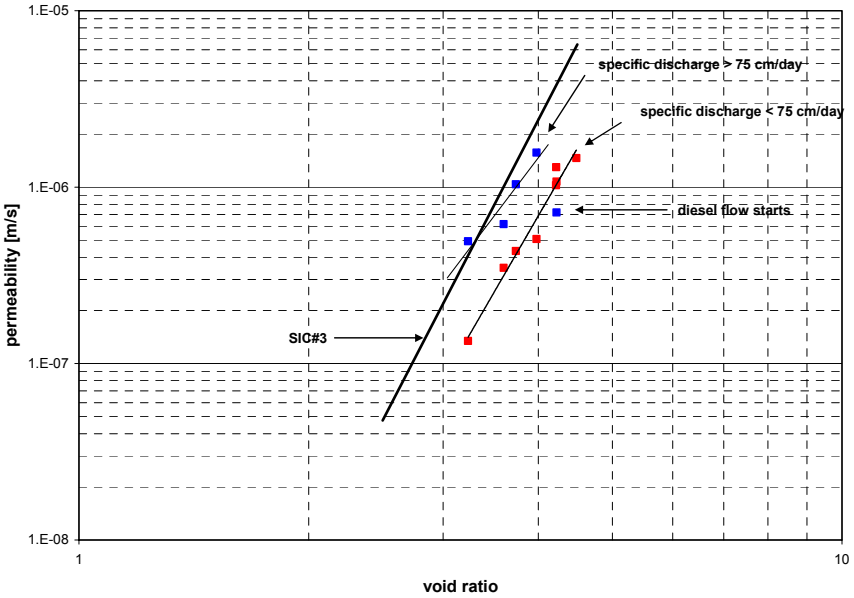

Figure 3.11 Permeability as function of void ratio SIC#4

The relation between permeability k in terms of [m/s] and intrinsic permeability is given by:

$$k = \rho_w g \frac{k_w^i}{\eta_w} \tag{3.8}$$

In Fig.3.11 the permeability's are given according to eq.(3.8). From that plot a ratio between α and β of 2.5 can be obtained. With the viscosities of the diesel fuel and water the ratio intrinsic permeability is k_{NAPL}^i / k_w^i=6.65. This means that the NAPL phase occupies the largest pores.

During the test diesel fuel and pore water that was flowing out the sample (the filtrate) was collected. After the test the total amount was 20 ml diesel fuel and 340 ml of pore water. With a density of diesel fuel of 824 g/l and water of 1000 g/l the diesel concentration by weight is 4.8%. The sample after the test was dried in the oven, as indicated in section 3.1, but with an additional first step: drying the sample in a 100 % humidity jar at 55 ^{o}C. In this way the diesel and other VOC's are evaporated from the sample without changing the water content. The measured diesel+VOC's concentration by weight of the pore water was 7.1%. The difference of 2.3% is related to the presence of mineral oils and PAHs in the original sample. From the analysis of Analytico on the original sample a mineral oil concentration of 3.3% weight dry solids (wt ds) and total PAH concentration of 1.7% (wt ds) was found (see section 4.6). With a pore fluid content after the test of 236 % (wt ds) the initial concentration of mineral oil and PAHs is (3.3+1.7)/2.36=2.1%.

Table 3.5 Coefficients SIC#4

A	***B***	***Z***	***C***	***D***
6.9	-0.17	12.36	2.1713E-11	7.4763

3.3.3 Test SIC#5

This test is performed with a gas (nitrogen) boundary on top of the sample and aimed at determining the "air entry value", which is important for gas bubble formation in sediments. The upper filter stone was saturated with water before the test. After consolidation by the weight of the top platen of 363 Pa three seepage loading phases were applied. During the first two seepage phases the water level was sufficiently high to do all six seepage discharges (see Table 3.3) for determining permeability.

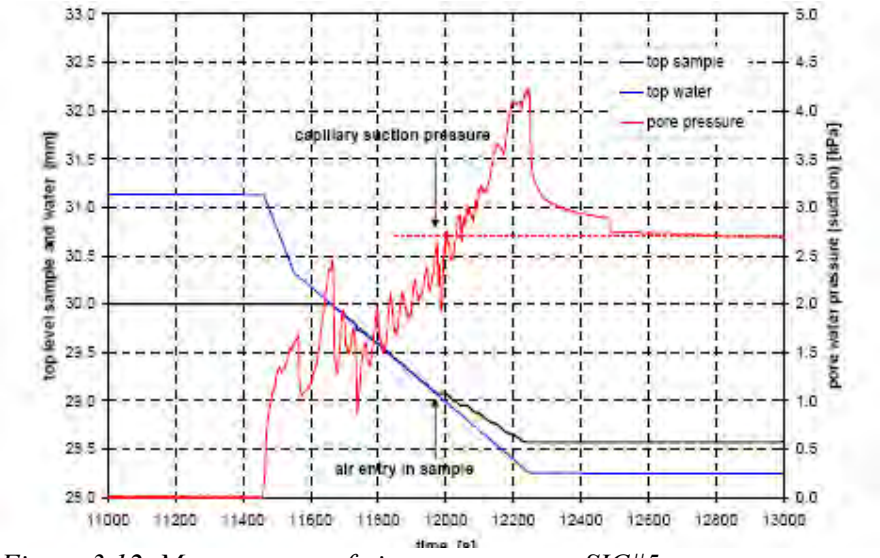

Figure 3.12 Measurement of air entry pressure SIC#5

The 3rd seepage phase was used to determine the "air entry value". This loading phase is shown in Fig.3.12, where the top level of water (blue line), the top level of the sample (black line) and the suction pressure in the drain system (red line) are plotted as function of time. The seepage discharge was started at 0.75 m/day, but reduced to 0.25 m/day after 100 seconds in order to get higher accuracy for the air entry value. At 11650 seconds the water level hits the top of the sample and the capillary force starts consolidating the sample. As long as the capillary force is less than the failure suction pressure of the menisci in the largest pores, the top sample must follow the water level. This forced displacement of the top level of the sample results in an increasing suction pressure in the drain system. At 11990 seconds, the top level of the sample is deviating from the water level, indicating that the menisci in the largest pores starts failing and nitrogen enters the sample. The corresponding capillary suction pressure is 2.69 kPa, which is also defined as the "air entry value". After this point the suction pressure is still increasing due to the capillary forces of the smaller pores. After 12250 seconds the maximum volume has been displaced by the pump and the seepage stops. The suction pressure is dropping to the level of the "air entry value". The capillary pressure can be related to the pore diameter with:

$$u_{cap} = 4\frac{\sigma \cos\alpha}{D_p} \tag{3.9}$$

in which u_{cap} is capillary pressure in [Pa], D_p is pore diameter, σ is surface tension in [N/m] and α is wetting angle on solid surface.

With a surface tension of 0.071 N/m and zero wetting angle (assuming water film on solid surface) the pore diameter corresponding to the air entry value of 2.69 kPa is 106 μm. For gas bubble formation in a sediment the air entry value should be larger then the pressure to squeeze away the sediment matrix. This condition is given by (Winterwerp & Van Kesteren, 2004):

$$p_g = Nc_u < p_{ae} \tag{3.10}$$

in which p_g is gas pressure inside bubble [kPa], p_{ae} is air entry value [kPa], N a constant ≈ 7.5 and c_u the untrained peak strength of the sediment [Pa].

With an air entry value of 2.69 kPa, the strength of the sediment must be smaller than 360 Pa for bubble formation. A larger strength will result in desaturation of the pore system. Given strength of 200 Pa of the wood layer (see Fig.3.6), bubble formation can occur and gas will be trapped in the sediment. However during consolidation the strength will increase rapidly, while the void ratio remains almost the same resulting in a small increase in air entry value. The results is that desaturation of the pore system will occur, which enables a pathway for gas releases.

The test is continued by external loading phases and seepage phases as indicated in Table 3.3. The relationship between effective stress and void ratio is given in Fig.3.13 and is similar to SIC#3 which fit is also shown. The permeability as function of void ratio is shown in Fig.3.14. The first two seepage phases, which has been applied before the nitrogen entered the sample, correspond to the SIC#3 relationship. Due to desaturation of the largest pores the permeability is changing and increasing above the SIC#3 relationship. The higher permeability is related to channeling effect in the largest pores. The coefficients for SIC#5 are listed in Table 3.6.

Table 3.6 Coefficients SIC#5

A	***B***	***Z***	***C***	***D***
5	-0.128	5.72	1.2154E-09	5.3727

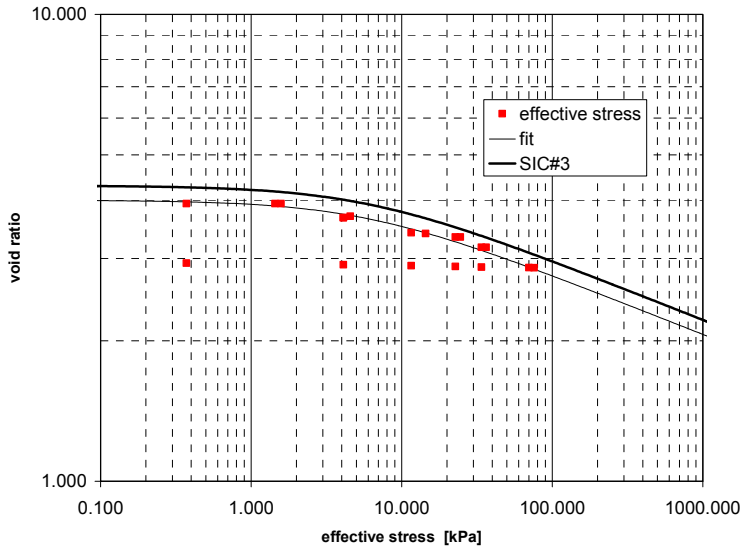

Figure 3.13 Effective stress as function of void ratio SIC#5

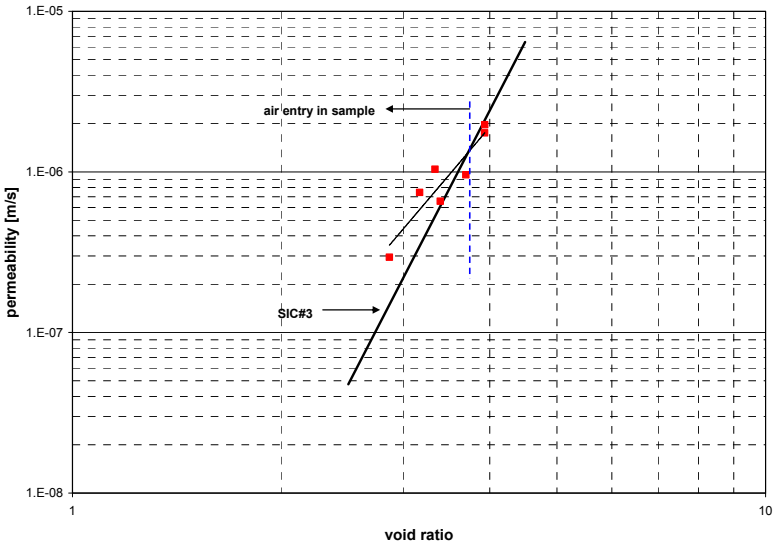

Figure 3.14 Permeability as function of void ratio SIC#5

4. Supplemental Analyses

The following analyses were conducted on the contaminated sediment:

- Gas content (methane and carbon dioxide) and gas production rates (4 temperatures) (WL|Delft Hydraulics);
- Vane tests and water content (WL|Delft Hydraulics);
- Particle size distribution (GeoDelft);
- Atterberg limits (plasticity and liquid limit) (GeoDelft);
- Sediment composition:
  - Water content (WL|Delft Hydraulics);
  - NAPL content (Analytico);
  - Organic content (OC) (GeoDelft, WL|Delft Hydraulics);
  - Carbonate content (GeoDelft);
  - NAPL content in sediment measuring PAHs and mineral oil (Analytico)
- TerrAtest on filtrate SIC test measuring PAHs, VOCs and mineral oil (Analytico).

4.1 Gas content and production rates

Two samples from the same batch, which has been used for the SIC tests, were placed in cell #1 and cell #2 of the gas facility at WL|Delft Hydraulics. A schematic set-up is shown in Fig.4.1. This facility measures methane and carbon dioxide that is present in the sediment, and anaerobic bacterial or chemical production rate as function of temperature. Methane is measured with a GC (FID). Carbon dioxide is measured by transforming it into methane with hydrogen via a Ni-catalyst. For calibration 2 standard gasses with 10 ppm and 1000 ppm of CH_4/CO_2 mixture (50%/50%) are measured each time samples are measured (default four times a day). Gas samples are taken from the head space of each cell. The carrier gas is nitrogen. When the concentration in the head space is in the order of 1000 ppm the cells are flushed with humid nitrogen in order to prevent drying of the sediment samples.

The sample in cell #2 was aimed at measuring chemical induced production rates, which was achieved by adding a bacteria killing agent (formaldehyde) after the degassing period and one week of bacterial activity. The sample in cell #1 was aimed at measuring both bacterial and chemical production rate as function of temperature: 10 ^{o}C and 20 ^{o}C. The samples were very soft and therefore placed on the bottom of the cell. The sample volume was 90 ml, resulting in a layer thickness of 18 mm.

Due to malfunction of the Ni-catalyst, carbon dioxide could not be measured. For production rates methane and carbon dioxide will be similar, however the initial concentration of carbon dioxide is not known and must be assessed with DELCON (see Ch. 6).

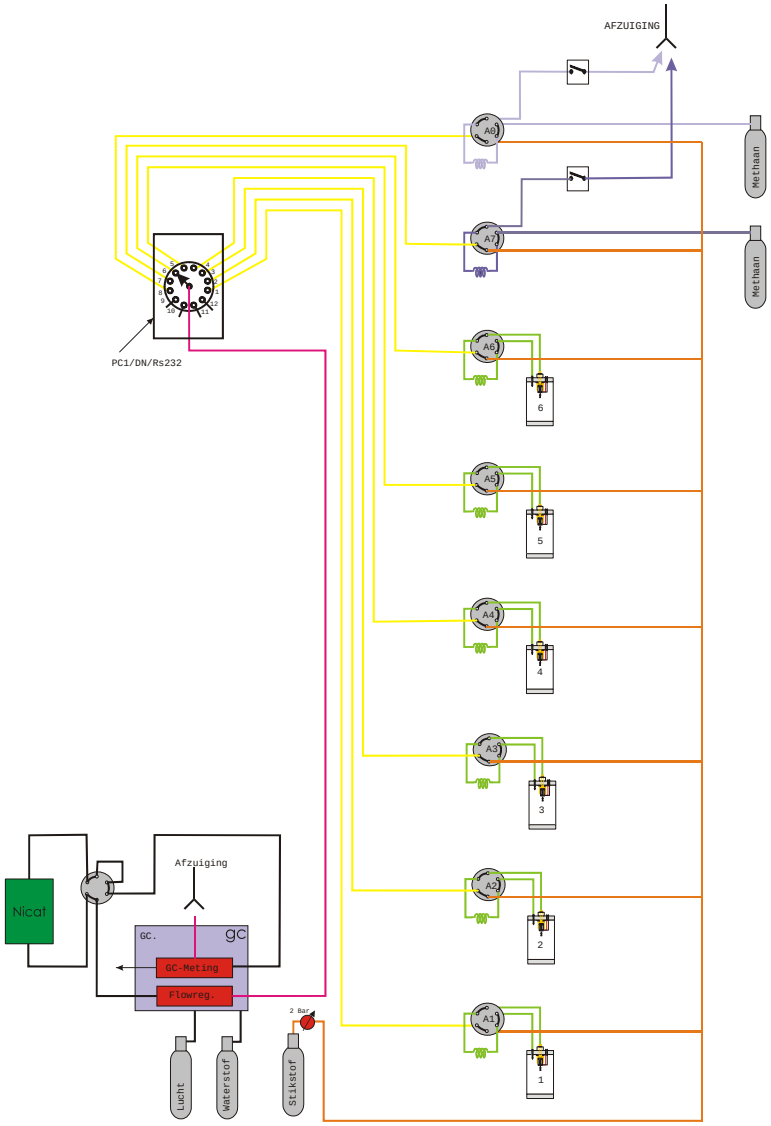

Figure 4.1 Test set-up gas facility

The results for methane at 10 ^{o}C are shown Fig.4.2 and Fig.4.3 as function of time for respectively cell #1 and #2. The measured data are fitted with the theoretical diffusion flux superimposed on a linear production rate. The fit parameters are the diffusion coefficient, the initial methane concentration and production rate and are given in Table 4.1. The results for cell #1 and #2 are similar, except that in cell #2 after 780 hours the methane production

rate reduces to zero due to the addition of bacteria killing agent (formaldehyde). In Fig.4.4 the methane production rate at 20 ^{o}C in cell #1 is shown. The only fit parameter is the production rate (see Table 4.1).

Production rates are measured as an increase in head space concentration in ppm CH_4 per hour. Given the amount organic matter in the sample of 67.4% (wt ds) (see Table 3.1) the production rate can be expressed in mmol CH_4 per gram OM per year. The DELCON model is based on the 2nd order degradation model of Middelburg (1989) which requires degradation rate of organic matter per year. These numbers are also given in Table 4.1 and plotted as function of temperature in Fig.4.5. The linear fit results in a critical temperature for bacterial activity of 6.76 ^{o}C.

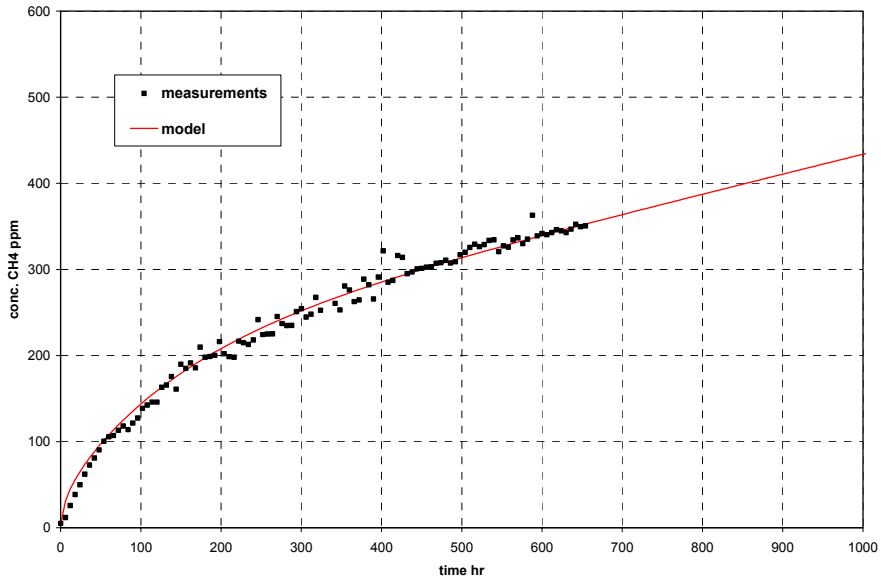

Figure 4.2 Concentration methane in headspace cell #1 at 10 ^{o}C

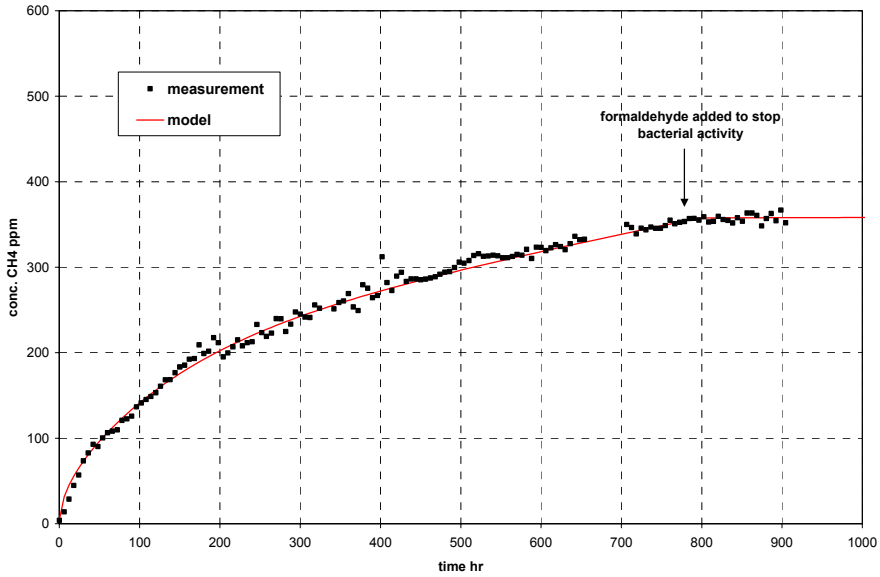

Figure 4.3 Concentration methane in headspace cell #2 at 10 ^{o}C

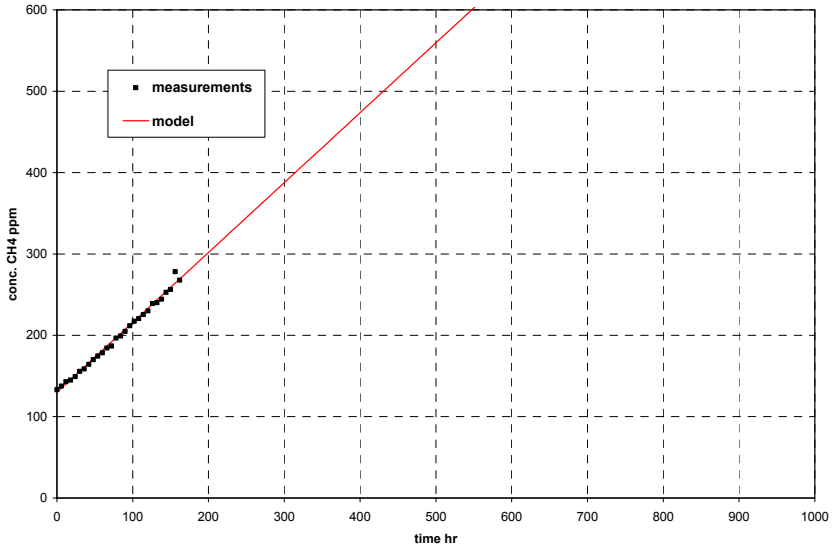

Figure 4.4 Concentration methane in headspace cell #1 at 20 ^{o}C

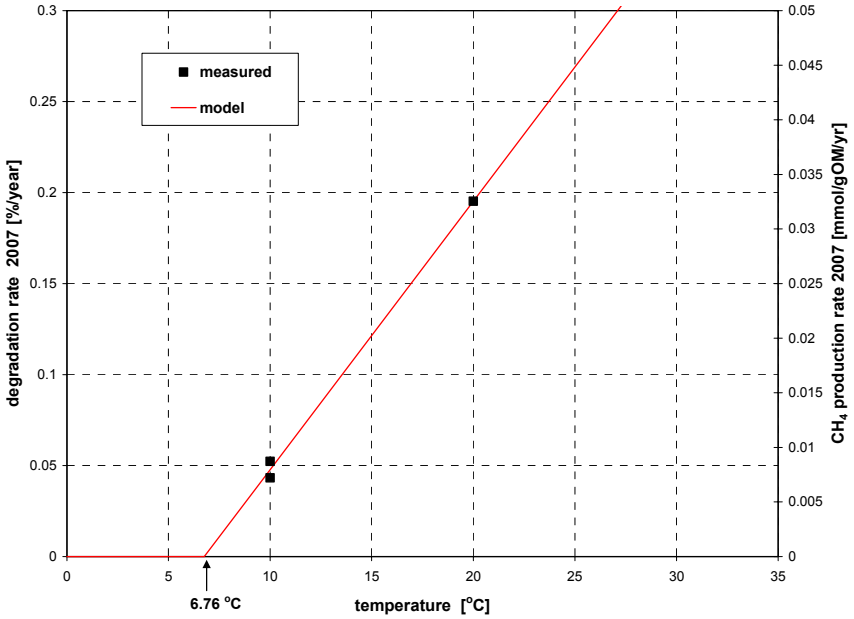

Figure 4.5 Degradation rate and gas generation rate as function of temperature

Table 4.1 Fit parameters CH_4 production tests

parameter	cell #1 10 °C	cell #1 20 °C	cell #2 10 °C
diffusion coefficient [m^2/s]	$1\ 10^{-9}$	$1\ 10^{-9}$	
initial concentration in headspace in ppm	204		207
initial concentration in pore fluid in mmol/mol	0.00209		0.00208
production rate in headspace ppm/hr	0.23	0.86	0.19
production rate in mmol/gOM/yr	0.00871	0.0325	0.00720
degradation rate of organic matter in % per year	0.0523	0.195	0.0432

4.2 Vane Tests

Vane tests[2] are performed on the sample used for SIC test #3 before and after the test. The vane tests are done with Haake M1500 rotoviscometer with vane elements FL100 and FL1000. The rotation speed was 0.512 rpm. The results are given in Table 4.2 and shown in Fig.4.6 (before SIC test) and Fig.4.7 (after SIC test). The wood chips and fibres affected the vane test, especially the sample after the test. That may have contributed to the continuous decay of the strength in the sample after the test. The failure in the sample was such that a duplicate test was not possible.

Table 4.2 Vane test results

Test	number	W %	c_u Pa	$c_{u,r}$ Pa
SIC #3 before test	1	411.1	196	39
SIC #3 before test	2	411.1	168	38
SIC #3 after test	1	247.9	39500	1800

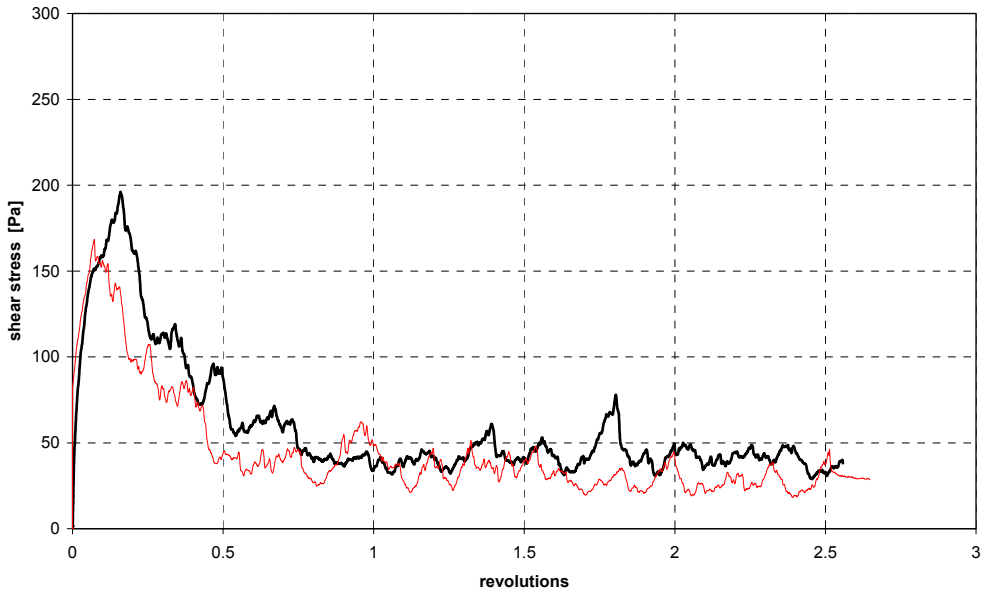

Figure 4.6 Vane test SIC#3 before test (in duplicate with vane element FL100)

[2] A vane test is a simple but efficient method to measure the yield stress among other properties of non-Newtonian fluids.

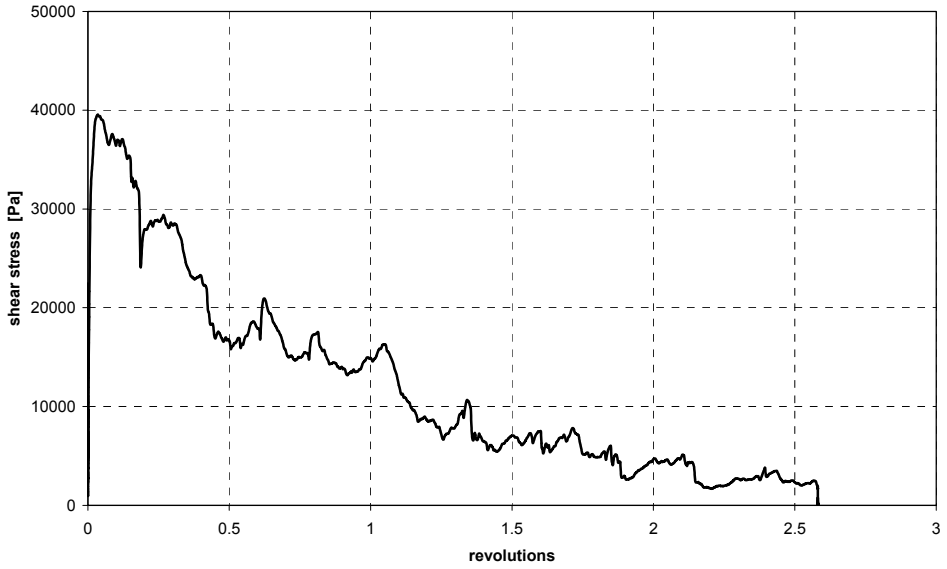

Figure 4.7 Vane test SIC#3 after test (with vane element FL1000)

4.3 Particle Size Distribution

The particle size distribution was determined by GeoDelft on the mineral fraction of the upper half of core sample from area 2 (see Fig.3.1): Sample 200 ft SE. The mineral fraction was obtained after drying at 1100 ^{o}C and was 44.3% of the total solids remaining after drying at 105 ^{o}C (see Table 3.1). The mineral solids were dry sieved down to 38 μm; the fraction smaller than 38 μm was measured with a Sedigraph. The result is shown in Fig.4.8. The clay content is 3.4 %, silt content is 21.9 %, and sand+gravel content is 74.7 % or respectively 1.5%, 9.7% and 33% of the total solids defined by drying at 105 ^{o}C.

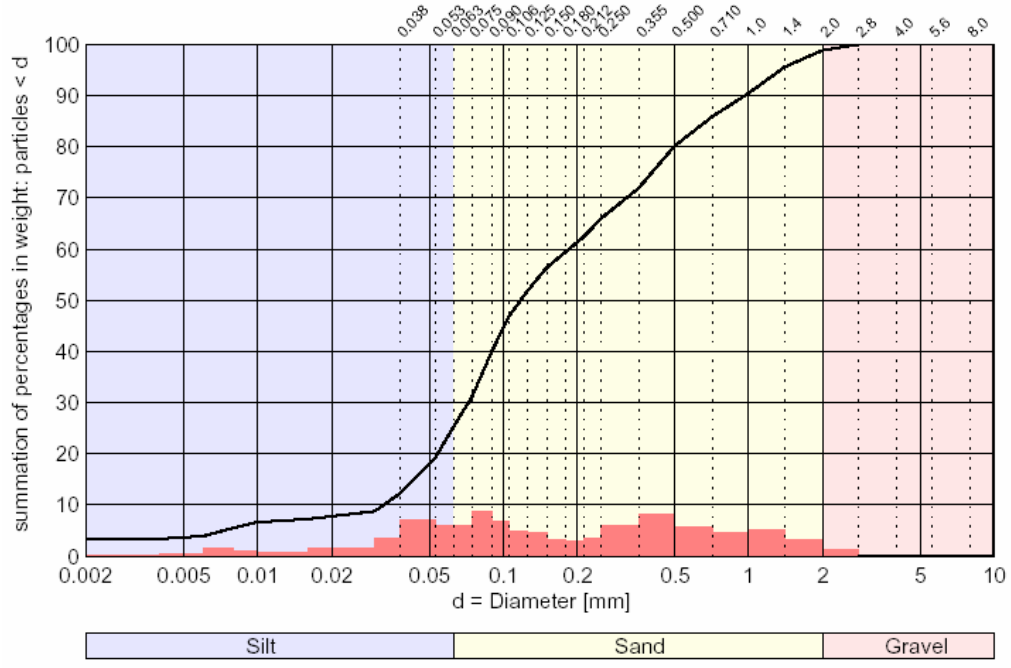

Figure 4.8 Particle Size Distribution contaminated wood layer after 1100 ^{o}C

4.4 Atterberg limits

The Atterberg limits couldn't be determined due to the high sand content in the mineral fraction and high organic content in the total solids. The cohesive nature is mainly determined by the organic (wood) fibre structure of the sediment and not by the clay fraction of the mineral part. The clay mineral content of the total solids is 1.5% (3.4% of 44.3%; see section 4.4). The behaviour is similar to peat soils in which fibre structure and reduced permeability by the clay fraction results in a cohesive behaviour. It must be noted that cohesive behaviour is related to the rate of pore water pressure dissipation when the sediment is loaded (see Winterwerp&VanKesteren, 2004)

4.5 Sediment composition

The water content, solid content, organic content, mineral content and carbonate content were measured by GeoDelft and WL|Delft Hydraulics and listed in Table 3.1 (section 3.1). The PAH's and petroleum hydrocarbons were measured by Analytico and are listed in Table 4.3. The sum PAH's and mineral oil is assumed to be in the NAPL phase, which yields a NAPL content of 5% by weight of dry solids (105 ^{o}C).

Table 4.3 Analysis Analytico

solid content	20.6	% m/m
PAH		
Naphthalene	5800	mg/kg ds
Acenapthalene	<5.0	mg/kg ds
Acenaphthene	2500	mg/kg ds
Fluorene	870	mg/kg ds
Phenanthrene	2800	mg/kg ds
Anthracene	1000	mg/kg ds
Fluoranthene	880	mg/kg ds
Pyrene	1100	mg/kg ds
Benzo(a)anthracene	390	mg/kg ds
Chrysene	280	mg/kg ds
Benzo(b)fluoranthene	230	mg/kg ds
Benzo(k)fluoranthene	90	mg/kg ds
Benzo(a)pyrene	370	mg/kg ds
Dibenzo(a,h)anthracene	25	mg/kg ds
Benzo(g,h,i)perylene	140	mg/kg ds
Indeno(123-c,d)pyrene	140	mg/kg ds
Total PAHs	17000	mg/kg ds
Petroleum Hydrocarbons		
C10-C40	33000	mg/kg ds
C10-C12	17.5	%
C12-C22	81.2	%
C22-C30	0.9	%
C30-C40	0.4	%

4.6 Contamination Filtrate SIC-test

The contamination in the filtrate of SIC test SIC #3 and SIC #4 are determined by Analytico and are listed in Table 4.4. The high mineral oil level in SIC #4 is due to the presence of diesel fuel that was used in the test as an upper boundary condition.

Table 4.4 Contamination level in filtrate of SIC #3 and SIC #4

		SIC #3	SIC #4
Soil analyses			
pH		7.1	7.8
pH-temperature	°C	17.9	18.1
EC (electrical conductivity temperature	°C	17.9	18.1
EC (25°C)	mS/m	12	<10
EC-temp. corr. factor (mathematisch)		1.171	1.166
Metals			
Barium (Ba)	µg/L	27	27
Cadmium (Cd)	µg/L	1.0	1.0
Cobalt (Co)	µg/L	2	1
Copper (Cu)	µg/L	110	170
Lead (Pb)	µg/L	35	64
Nickel (Ni)	µg/L	270	460
Zinc (Zn)	µg/L	940	1200
Benzene	µg/L	0.8	
Toluene	µg/L	0.9	
o-Xylene	µg/L	0.2	
m+p-Xylene	µg/L	0.4	
Xylenes (sum)	µg/L	0.6	
1,2,4-Trimethylbenzene	µg/L		87
Phenols			
o-Cresol	µg/L	0.76	
Cresol (som)	µg/L	0.76	
2,4-Dimethylphenol	µg/L	0.65	
2,5-Dimethylphenol	µg/L	1.2	2.1
2,6-Dimethylphenol	µg/L	3.3	
3,4-Dimethylphenol	µg/L	0.08	
o-Ethylphenol	µg/L	1.6	
2,3/3,5-Dimethylphenol + 4-Ethylphenol	µg/L	6.7	
PAH			
Naphthalene	µg/L	0.4	
Acenapthalene	µg/L	0.2	
Acenaphthene	µg/L	0.07	9.9
Fluorene	µg/L	0.56	12
Phenanthrene	µg/L	0.24	2.5
Anthracene	µg/L	0.51	3.0
Fluoranthene	µg/L	0.7	7.0
Pyrene	µg/L	1.2	
Benzo(a)anthracene	µg/L	0.87	
Chrysene	µg/L	2.2	
Benzo(b)fluoranthene	µg/L	1.8	
Benzo(k)fluoranthene	µg/L	0.2	
Benzo(a)pyrene	µg/L	1.3	
Dibenzo(a,h)anthracene	µg/L	0.9	
Total PAK VROM (10)	µg/L	9.9	18
Total PAH EPA (16)	µg/L	11	35
Chlorophenols			
Pentachlorophenol	µg/L	0.33	
Miscellaneous			
Biphenyl	µg/L		11
Petroleum Hydrocarbons			
C10-C16	µg/L		37000
C16-C22	µg/L		41000
C22-C30	µg/L		5500
C30-C40	µg/L		260
(som C10 - C40)	µg/L		84000

5. Schematization of Ashland Site

5.1 Geological Description

The regional and site geology is described in RI report (URS, 2006). The Site geological units are given in Figure 5.1, which shows a typical cross section (C-C') from SE to NW. Unconsolidated glacial deposits consists of the Miller Creek Formation and Copper Falls Formation and are overlying Precambrian aged sedimentary bedrock (Oronto sandstone). The Miller Creek Formation is a fine-grained clayey silt to silty clay formed by lacustrine deposits and glacial till deposit. The Copper Falls Formation consists mainly of gravel, sand and silty sand with silty clay and clay lenses. The low permeability of the Miller Creek Formation acts as an aquitard for the Copper Falls aquifer. Close to the Chequamegon Bay shoreline the excess pore pressure at the base of the Miller Creek Formation is 12 feet or more above Lake Superior water level (602 ft).

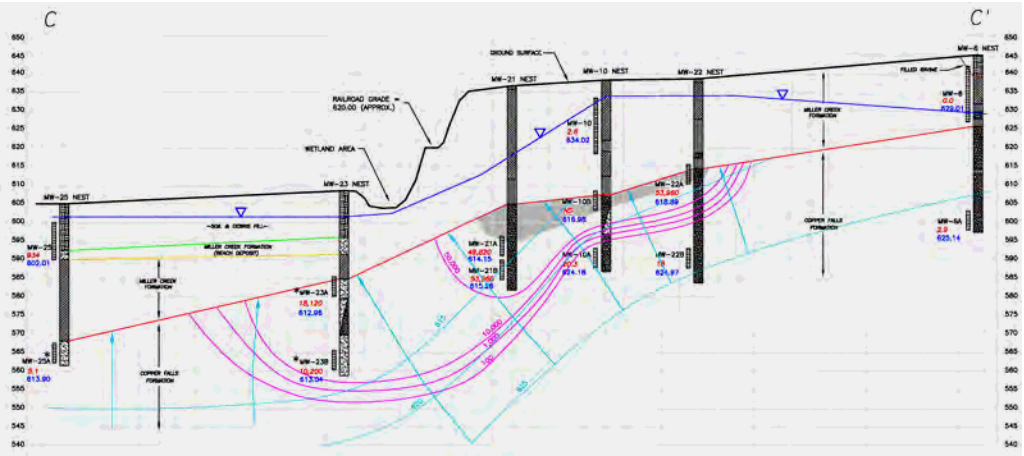

Figure 5.1 Site geological units in Cross Section C-C' (from RI-report fig. 3-4)

5.2 Bathymetry

In Fig.5.2 the bathymetry of the Ashland site is given together with the location of the sheet pile wall for the CDF. Initially the sheet pile wall was located at 2500 ft Northing, but in order to increase capacity the sheet pile wall was shifted 50 ft northward. From the bathymetry the hypsometric curve, i.e. surface area as function of depth, can be determined and is given in Fig.5.3. For the DELCON computation the hypsometric curve is schematized with 5 boxes, with a total volume that equals the area of the hypsometric curve. By using the hypsometric curve each box is bounded by two depth contours (see Table 5.1). At the sheet pile wall all contour

lines coincide. In table 5.1 also the bottom level, surface area of each box, cumulative area, and volume are given.

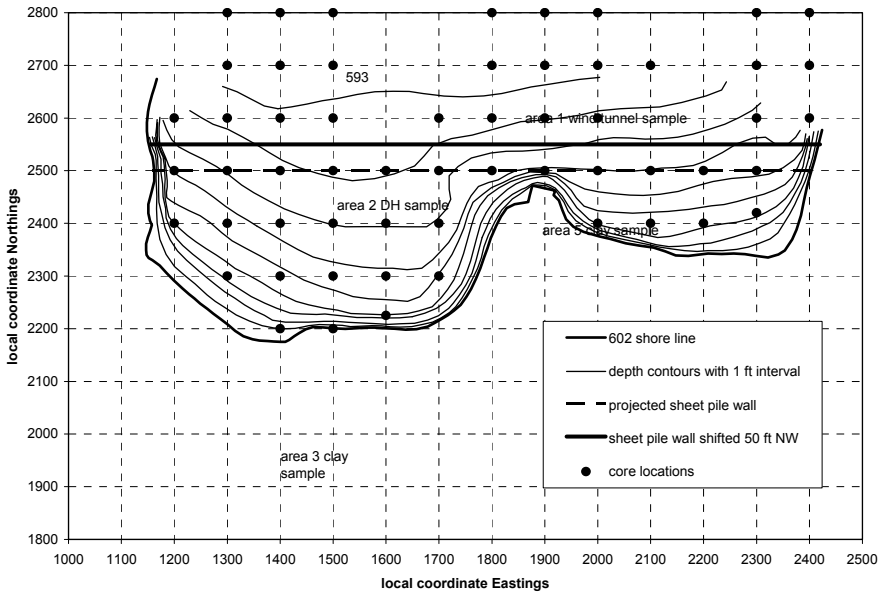

Figure 5.2 Bathymetry and core locations Ashland site

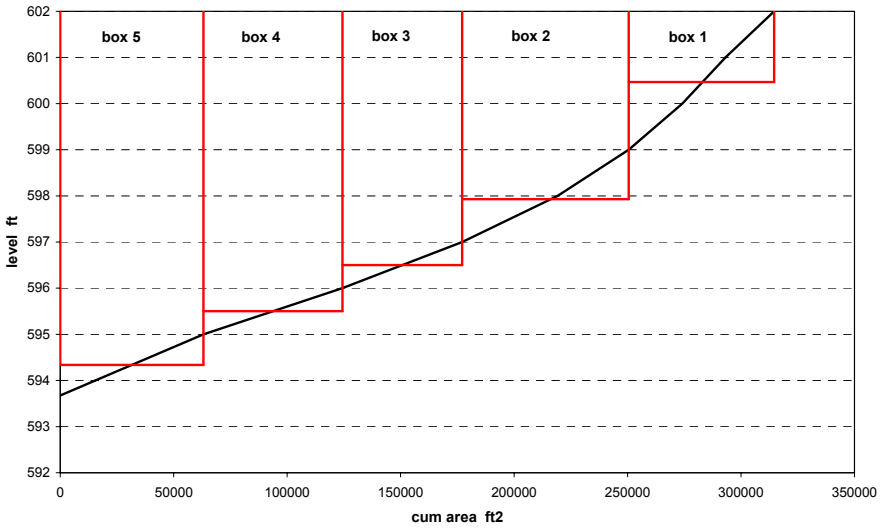

Figure 5.3 Hypsometric curve and schematization into 5 boxes

Table 5.1 Box schematization

box	depth contours [ft]	bottom level [ft]	surface area [ft^2]	cum. surface area [ft^2]	volume [yd^3]
#1	599 - 602	600.46	64098	314575	3647
#2	597 - 599	597.93	73379	250477	11070
#3	596 - 597	596.50	52716	177098	10738
#4	595 - 596	595.50	61291	124382	14755
#5	- 595	594.34	63091	63091	17907
sum			314575		58117

5.3 Stratigraphy

The core information in the locations indicated in Fig. 5.2 enables quantification of the stratigraphy in the CDF area between the shore line and sheet pile wall. There are 5 sediment layers identified from the core logs:

1. contaminated wood layer (WD)
2. sand layer (SD): Miller Creek Formation beach deposit
3. silt layer (SI): Miller Creek Formation silt deposit
4. clay layer (CL): Miller Creek Formation clay deposit
5. sand layer (CF): Copper Falls Formation

For each box the thickness of each layer has been assessed by averaging between contours of each box. The wood layer is the most compressible layer and will determine mainly the settlement when loaded with dredged material and when capped with sand. The thickness of the wood layer is shown in Fig.5.4. It shows that within the CDF area the estimated wood layer thickness roughly follows the bathymetry. Therefore the box schematization based on depth contours will be able to represent the effect of wood layer compression.

The result for the schematized stratigraphy is shown in Fig.5.5 and listed in Table 5.2. The top of the Copper Falls formation is assumed to be the base of the stratigraphy in the DELCON computations and is set to a level of 547 ft in all boxes.

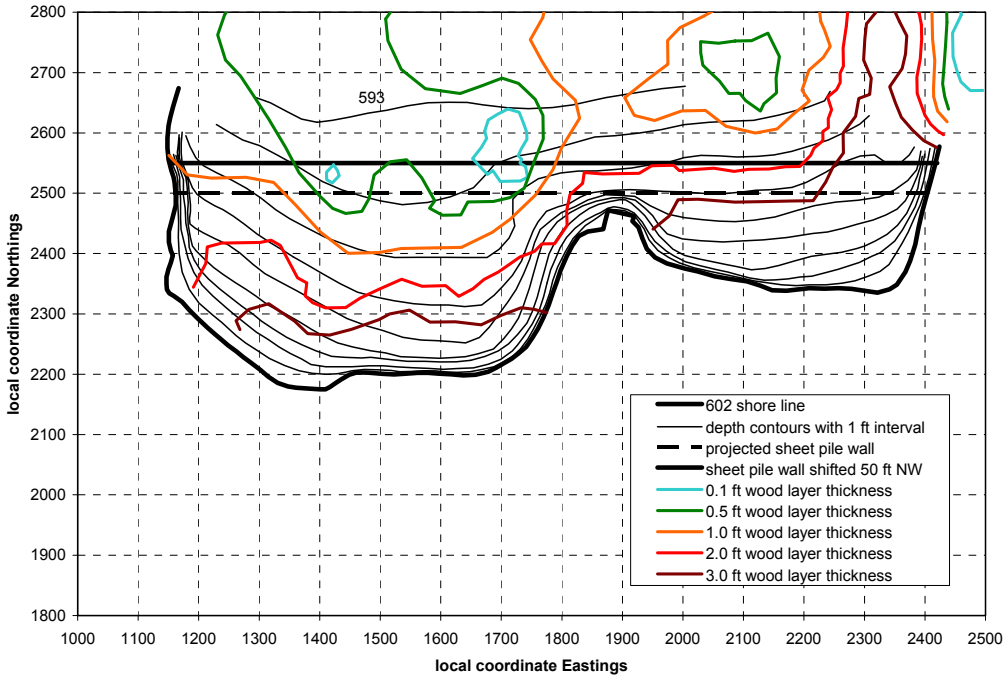

Figure 5.4 Wood layer thickness

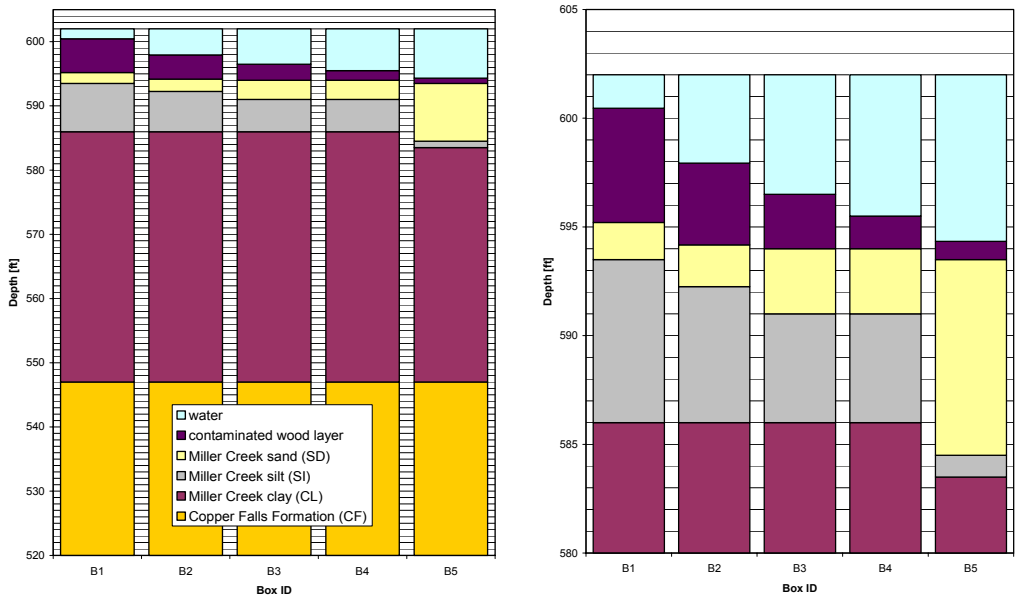

a) all layers *b) detail top layers*

Figure 5.5 Schematized stratigraphy

Table 5.2 Schematized stratigraphy

top unit [ft]	B 1	B 2	B3	B4	B5
water	602	602	602	602	602
wood layer	600.46	597.93	596.5	595.5	594.34
MC sand	595.21	594.18	594	594	593.5
MC silt	593.5	592.25	591	591	584.5
MC clay	586	586	586	586	583.5
CF sand	547	547	547	547	547

5.4 Material properties sediment layers

5.4.1 Miller Creek Clay

For the properties of the Miller Creek clay, samples from area 3 and 5 (Figure 3.1) were analyzed. The available properties were Atterberg limits (LL, PL and PI), particle size distributions and water content. The plasticity index (PI=LL-PL) is given in Fig.5.6 as function of the clay content. It shows that both area 3 and 5 samples coincide on a straight line. The gradient is defined as the activity A of the clay fraction and is about 0.7. Given a constant activity in different samples, the consolidation characteristic can be obtained from one oedometer test. This test was done by SET on a sample from area 5 (see Appendix A). The void ratio as function of effective stress can be fitted with eq.(3.2), which is shown in Fig.5.7a. The permeability is determined from the consolidation coefficient given in Appendix A. The results are shown in Fig.5.7b. The back calculation of the permeability from the consolidation coefficient is only allowed on the compression line that corresponds to the 2 lower void ratio's in Fig.5.7a. Therefore the power law according to eq.(3.3) is fitted on these 2 points. The fit coefficients *A,B,Z,C* and *D* are listed in Table 5.3. The consolidation coefficient at the in-situ effective stress of about 100 kPa or 14 psi is 9.8 10^{-7} m^2/s (see Appendix A). With eq.(3.5) and layer thickness of 39 ft (see Fig.5.5a) the time scale for consolidation of the Miller Creek clay is about 5 years.

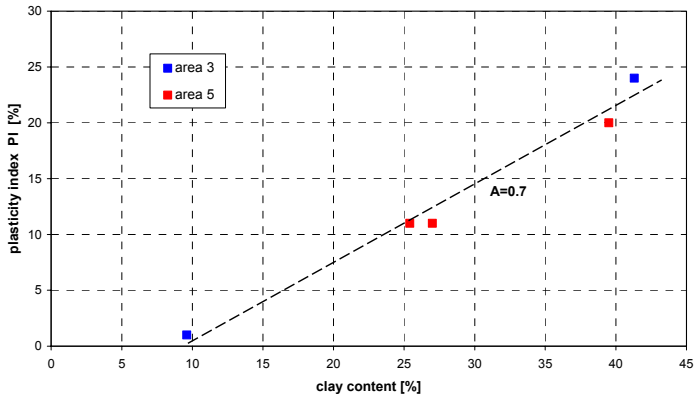

Figure 5.6 Activity plot Miller Creek clay

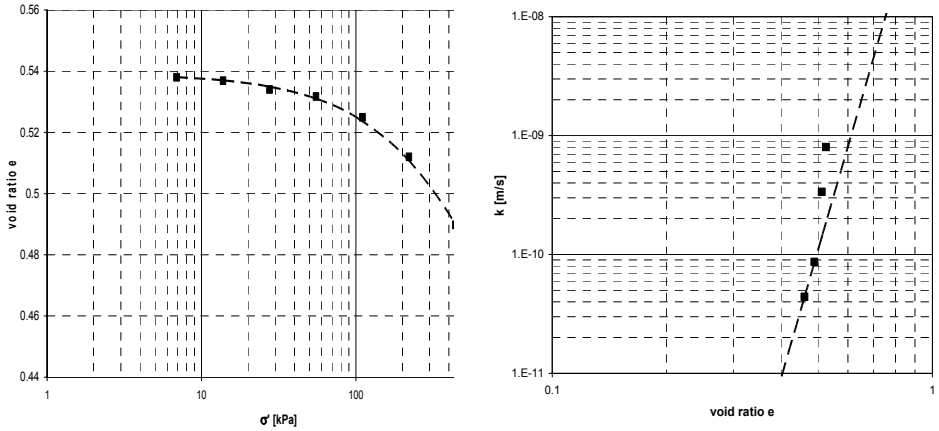

a) effective stress *b) permeability*

Figure 5.7 Effective stress and permeability as function of void ratio

5.4.2 Miller Creek Silt

For Miller Creek silt, properties are obtained from the core information in the locations indicated in Fig.5.2. From the physical properties (water content, depth; see URS report 2007) an assessment can be made of the consolidation properties. From the depth an effective stress level can be assessed assuming a consolidated state of the silt skeleton. From the water content the porosity and void ratio can be calculated. However when the silt skeleton is dominating the effective stress is determined mainly by the void ratio with respect to the silt skeleton. The same holds for the permeability. Therefore an assessment is made of the sand content in each Miller Creek silt sample. From the sediment phase theory (Winterwerp and Van Kesteren, 2004) a relation is found between the change in void ratio as function of sand content. With the computed effective stress level for each sample and the power law in eq.(3.2), the void ratio with respect to the silt skeleton can be

expressed in the coefficients A, B and Z. The void ratio with respect to silt skeleton can also be expressed in the actual void ratio and the sand fraction. The coefficients A, B and Z can be optimized in a way that the measured void ratio and computed sand fraction correspond to the sediment phase theory. The result is shown in Fig.5.8 for coefficients: A=1.5, B=-0.15 and Z=3.

The permeability is determined with Kozeny Karman formulation, given by:

$$k = \frac{g}{\upsilon}\frac{1}{k_0}\frac{e_{si}^3}{1+e_{si}}\frac{1}{S_v^2} \;;\; e_{si} = \frac{1+e}{\xi_{si}} - 1;\; S_v = \frac{N}{D_{10}} \;;\; N \approx 9.5 \;;\quad k_0 \approx 12.5 \quad (5.1)$$

in which D_{10} the diameter with 10% lower, e_{si} void ratio silt and ξ_{si} the silt fraction.

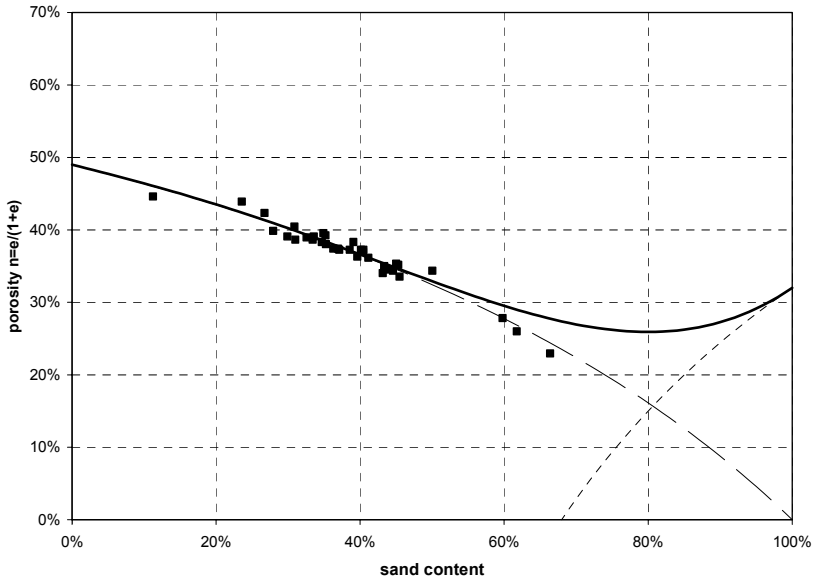

Figure 5.8 Optimization coefficients A,B and Z with sediment phase theory

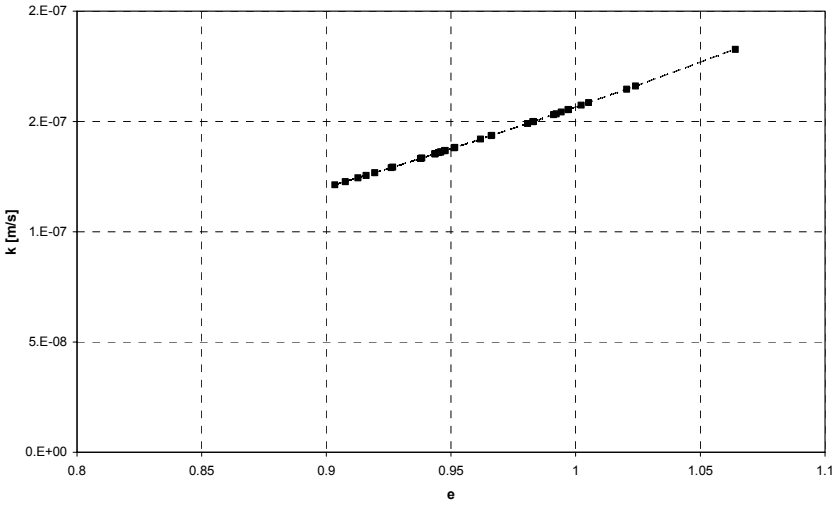

Figure 5.9 Permeability as function of void ratio Miller Creek silt

With a D_{10} of 6 μm the permeability is calculated as function of void ratio and plotted in Fig.5.9. The data is fitted with the power law function eq.(3.3): C=1.56 10^{-7}, D=2.507 (see also Table 5.3).

5.4.3 Miller Creek Sand

In a similar way as the Miller Creek silt, the coefficients are determined for the Miller Creek sand. In this case it is assumed that the sand skeleton dominates the consolidation behaviour, with a constant porosity with respect to the sand fraction. The measured data is shown in Fig.5.9 and correspond to the coefficients: A=2.5, B=-0.18 and Z=237.7. The permeability is determined with Kozeny Karman formulation eq.(5.1) and plotted in Fig.5.10 for a D_{10} of 80 μm. The coefficients of the power law function are: C=3 10^{-5}, D=2.621 (see also Table 5.3).

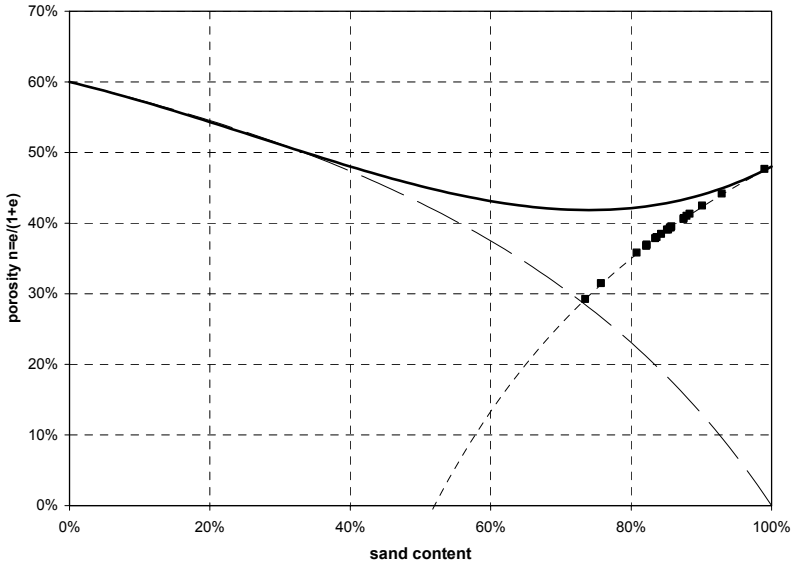

Figure 5.10 Optimization coefficients A,B and Z with sediment phase theory

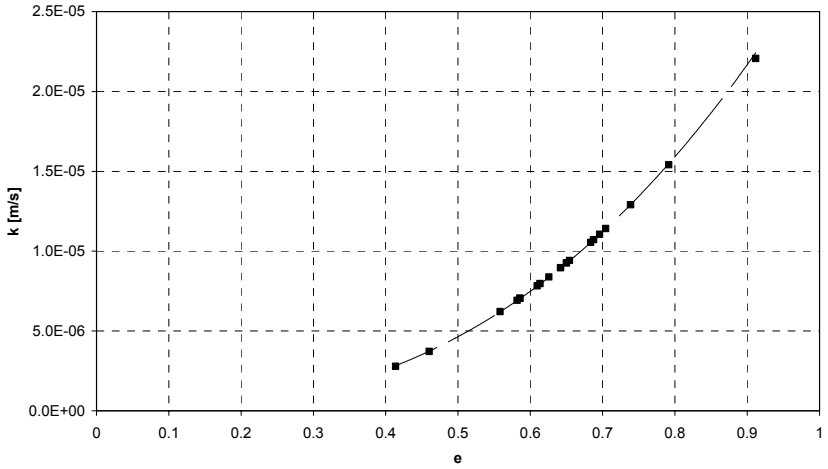

Figure 5.11 Permeability as function of void ratio Miller Creek sand

5.4.4 Contaminated Wood Layer

In this study only samples of the contaminated wood layer from area 2 (see Fig.3.1) has been tested for consolidation properties (see Ch.3). These properties were determined on the fraction smaller than 10 mm with a solid content (105^{o}C) of 19.6% (see Table 3.1). The total sample solid content was 23.1% with a 33% sand in the solids (see section 4.3). However the averaged solid content of the wood layer is 44.9%. It is assumed that the variation in solid content of the wood layer is caused by difference in the sand fraction. In order to get the averaged solid content of 44.9% a sand content of 63.9% is required. The addition of sand changes the void ratio's proportionally and therefore the coefficients for permeability and effective stress as given in Table 3.4 must be corrected. The corrected coefficients are listed in Table 5.3 together with the corrected densities, void ratio, NAPL content and organic content. It is known that in the wood layer near shore large logs are piled up in such a fashion that they form a skeleton which is able to partly bear the load of the dredged slurry. This may result in less consolidation of the wood layer. Due to lack of information about log concentration it was decided to do the DELCON simulations without the effect of logs.

5.4.5 Dredged Wood Layer Slurry

The dredged wood layer has the same effective stress and permeability relation with void ratio except that the deposition void ratio is higher and the Z value is close to zero (0.02).

For hydraulic dredging the solids content was set at 18% (see section 6.1), which corresponds to a void ratio of 8.58 with a solid density of 1889 kg/m^3 (see Table 5.3). With the coefficients in Table 5.3 for the dredged wood layer an effective

stress of 0.23 Pa and permeability of 0.21 m/s. The very low effective stress indicates a regime of hindered settling with different settling velocities with an average of 2 cm/s. In this settling regime sand particles will segregate from the wood material. DELCON assumes a non-segregating slurry. The minimum possible solids content is 28% or maximum void ratio of 4.867 (see Table 5.3), which corresponds to an effective stress of 21 Pa and a shear strength of 10 Pa (see Fig.3.6). This shear strength is sufficient to keep all particles in suspension.

For mechanical dredging the solids content was set at 40% (see section 6.1), which corresponds to a void ratio of 2.81 and effective stress of 1.46 kPa or shear strength of 0.7 kPa.

5.4.6 Cap Material

The particle size distribution of the cap material was measured by Soil Technology and is shown in Fig.5.12. For the effective stress void ratio relation the same coefficients are applied as for the Miller Creek sand, but with a lower void ratio: A=2.0, B=-0.18 and Z=237.7 (see also Table 5.3). The permeability was also measured by Soil Technology at a void ratio of 0.563: $k=10^{-4}$ m/s. For the relation between permeability and void ratio Kozeny-Karman formulation eq.(5.1) was used with a D_{10} of 200 μm in order to fit the measured permeability. The relation is plotted in Fig.5.13. The coefficients of the power law function are: $C=4.486\ 10^{-4}$, D=2.611 (see also Table 5.3).

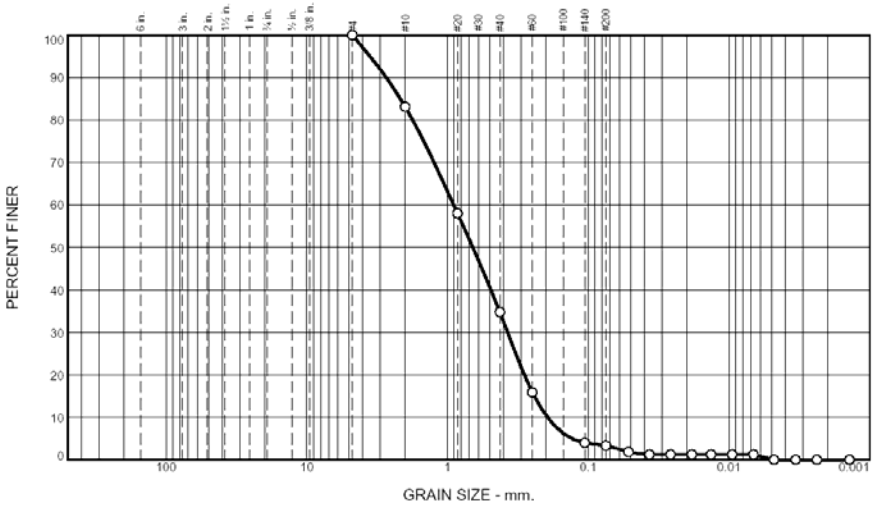

Figure 5.12 Particle size distribution cap material (source URS)

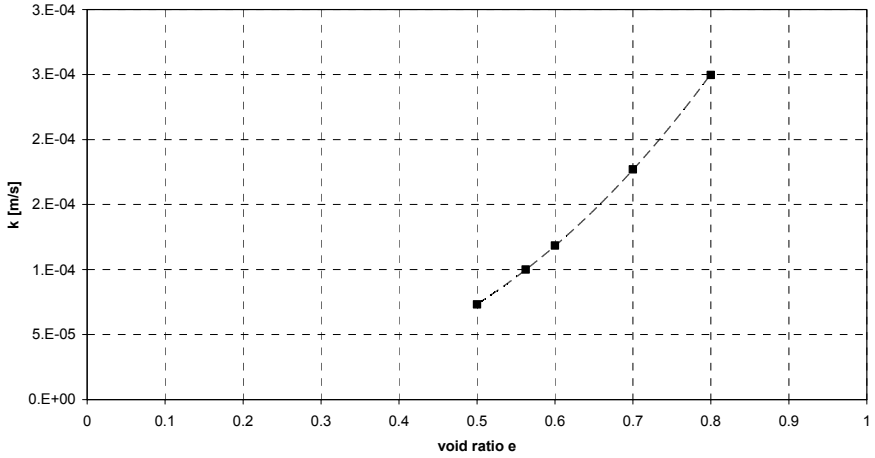

Figure 5.13 Gas generation test set-up

Table 5.3 Properties sediment layers for DELCON

parameter	MC clay	MC silt	MC sand	wood layer	dredged wood	cap
A	1.72	1.5	2.5	2.95	2.95	2
B	-0.18	-0.15	-0.18	-0.128	-0.128	-0.18
Z	629.8	3.0	237.7	5.716	0.0	237.8
C	$2.328\ 10^{-7}$	$1.565\ 10^{-7}$	$3.0\ 10^{-5}$	$3.368\ 10^{-9}$	$3.368\ 10^{-9}$	$4.486\ 10^{-4}$
D	11.061	2.507	2.621	8.351	8.351	2.611
e_0	0.539	1.271	0.934	2.360	4.867	0.747
ρ_w kg/m^3	1000	1000	1000	1000	1000	1000
ρ_s kg/m^3	2650	2650	2650	1889	1889	2650
ρ_{NAPL} kg/m^3				1124	1124	
org. content %	0	0	0	24.41	24.41	0
NAPL content %	0	0	0	1.25	1.25	0

5.5 Temperature

There are limited surface water temperature data available for the Ashland site area. Water temperatures measurements were made at the Ashland site in June 2005 (see Fig.5.14). However, cooling water intake temperatures are available over the period 2004-2006 from the Xcel Energy power plant in Ashland about one mile from the Site. The Ashland site temperature data from June 2005 were compared with the surface temperature water data from Stryker Bay (Duluth, MN) (Van Kesteren, 2002) (Fig 5.15). This temperature distribution curve is based on 11 years averaged data from 1991 until 2001. The Ashland site temperatures correspond well with the surface temperature water function developed from Stryker Bay. The Xcel Energy

intake water temperatures are somewhat lower in summertime and higher in winter time. This is caused by the 10 m water depth of the intake. It was concluded that based on the available data the existing surface water temperature function in DELCON can be applied for the Ashland site.

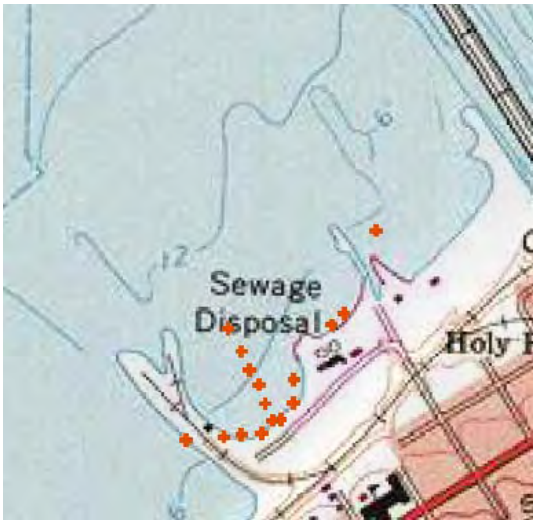

Figure 5.14 Locations surface water temperatures June 2004

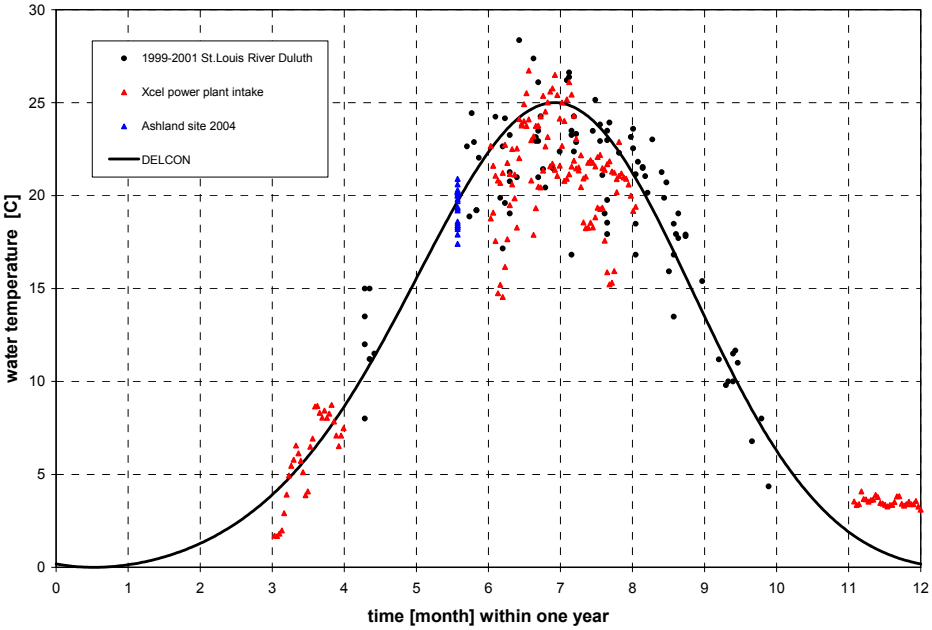

Figure 5.15 Temperature function Stryker Bay and temperature data Ashland site

6. DELCON Simulations

6.1 Alternatives remediation

URS defined four potential sediment remedial alternatives for the Ashland site:

Alternative #1:
No action.

Alternative #2:
Dredge sediment outside sheet pile with 6" overdredge and put dredged slurry in CDF between sheet pile wall and Ashland shoreline. The dredged slurry will be capped with sand of variable thickness: 2, 3.5, 5.2 and 7 ft (due to conversion factors different layer thicknesses were computed except the 2 ft). Dredging options include mechanical dredging at high solids (40% solids) and hydraulic dredging at low solids (18% solids). For this simulation, the dredging is assumed to occur for 6 months of operation per year with 5 working days in a week and 10 hrs per day. The production rate is about 60 cy/hr, which yields a weekly averaged production rate of 428 cy/day.

With the original location of the sheet pile wall at the 2500 ft coordinate vertical (see Fig.5.2) the total dredged volume was 73,771 cy, which corresponds to the revised clean-up goal of approximately 10 ppm TPAH. The shift 50 ft northwards reduces the dredging volume by 4,260 cy to 68,857 cy. This is still more than the nominal capacity of the CDF of 58,117 cy, but due to consolidation will fit in the CDF.

Alternative #3a:
Dredge sediment to a depth of 4 ft and cap the whole dredged area with sand with variable thickness: 1, 2, 3, 4 and 5 ft. The dredging rate is the same as in alternative #2. The model was used to determine what thickness of cap is required reach pre-dredge bathymetry after capping and consolidation.

Alternative #3b:
Dredge the contaminated wood layer to a depth of 2 ft and store it on site or landfill offsite and cap the whole dredged area with sand with variable thickness: 1, 2, and 3 ft. In between the cap and contaminated wood, a geotextile layer with activated carbon will be placed. Note that the carbon mat is for control of dissolved phase contaminants and not NAPL The dredging rate is half of alternative #2.

Alternative #4:
Dredge all sediments with PAHs above approximately 10 ppm. This means dredging to a depth of 10 ft or more and backfill with thin cap of sand or native clean sediment.

The DELCON simulations are done for alternatives #2 and #3.

6.2 Timeline

In the DELCON simulations the present situation before remediation is computed in a way that the present levels of in-situ layers are simulated. Therefore the simulation must follow the timeline of historical events at the site as shown schematically in Fig.6.1. The timeline of the simulations starts in 1650 AD with the placement of Miller Creek deposits (clay, silt and sand) on top of the Copper Falls Formation at a level of 547 ft. The Miller Creek clay is placed close to consolidation as one layer. The Miller Creek silt and sand are placed in 30 years. The period in between 1680 AD and the start of lumber activities at the site in 1884 AD are used to adjust the numerical simulation to the boundary conditions. In the period of 55 years from 1884 until 1939 AD lumber and tar residues are deposited forming the contaminated wood layer. Sedimentation of native sediment after 1939 is very limited (less than 10 cm) and therefore not included in the simulations.

The dredging activities were assumed to occur in 2007 AD from May 1st until October 31st. The capping activities were assumed to occur in 2008 AD from May 1st until October 31st. The simulations are continued until 2100 AD.

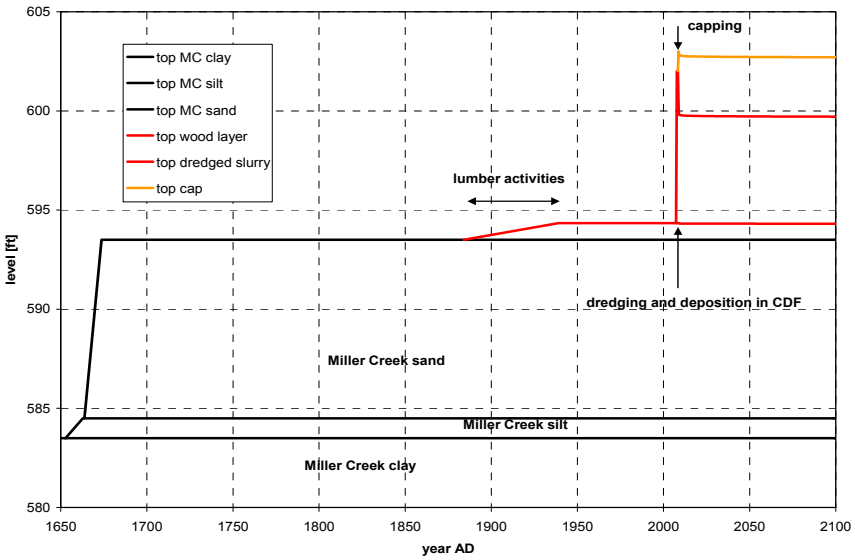

Figure 6.1 Timeline Ashland site (alternative #2 box B5)

6.3 Boundary Conditions

The lower boundary of the DELCON simulation is the Copper Falls Formation, which acts as an aquifer. Therefore, the lower boundary at a level of 547 ft is a drained boundary both for pore fluids and dissolved gasses. An excess pore pressure at the lower boundary is set at 12 ft water column with respect to water level in the bay.

In alternative #2 with a CDF, the top of the dredged slurry will be filled up to about 603.6 ft in order to store all the dredged material. Drains will be placed in the top of the slurry and the slurry covered by a membrane (see Fig.6.2). The cap on top of the membrane has its own drainage. The hydraulic head at the upper boundary of the dredged slurry is kept at 602 ft. Because there is no connection between the pore fluids of the cap and the slurry, the total weight of the cap, including pore water, act as vertical load for consolidating the slurry.

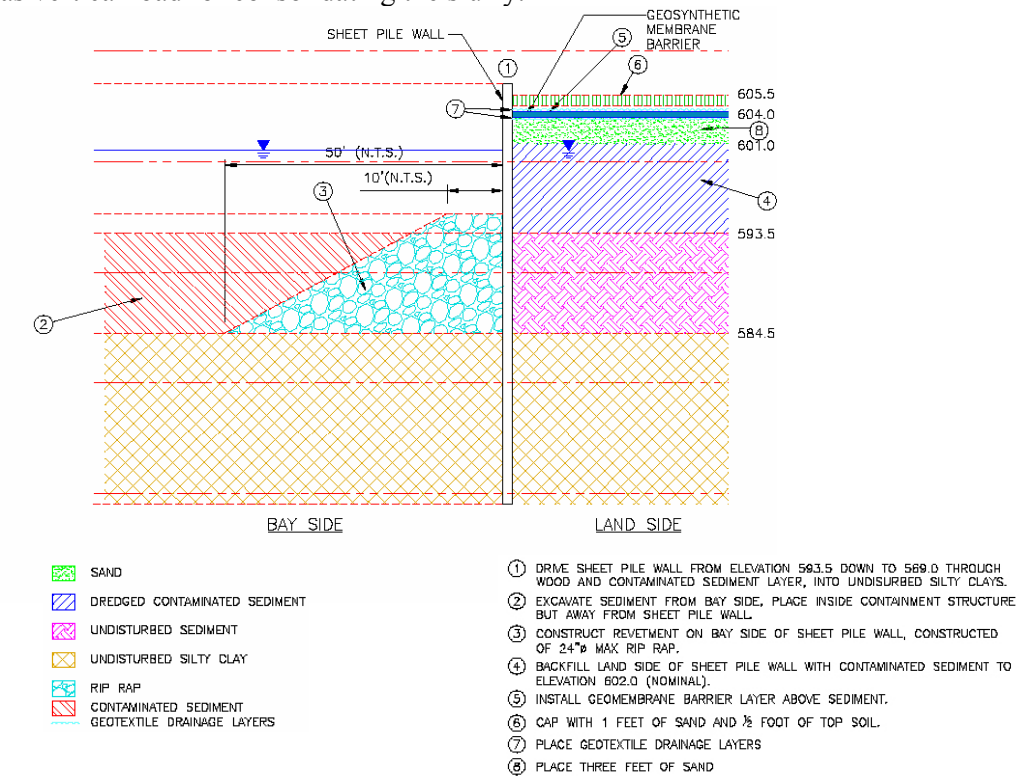

Figure 6.2 CDF cross section at sheet pile wall (alternative #2)(conceptual: source URS)

In alternative #3a and #3b the upper boundary condition is drained with the hydraulic head equal to the lake water level of 602 ft.

The generation of gas is a kind of internal time boundary that supplies at a certain rate of dissolved methane and carbon dioxide to the pore water and NAPL if present. There is only information about gas generation of the contaminated wood layer. Furthermore the organic content in the contaminated wood layer is very high and therefore only that layer is generating methane and carbon dioxide in the DELCON

simulations. The quantities of both gasses in mol/hr are assumed to be equal. The production rate of gas however will decrease over time. The second order degradation model of Middelburg (1989) is used in DELCON and is given by (see Winterwerp and Van Kesteren 2004):

$$\frac{\mathrm{d}\xi^{OM}}{\mathrm{d}t} = -k\left(t\right)\xi^{OM} \tag{6.1}$$

where ξ^{OM} is the content of organic matter in the total solids [kg/kg], t is time [year] and k the time-dependent decomposition decay function, given by:

$$k\left(t\right) = f(T)\; k_1\left(t_{age}+t\right)^{k_2} \quad [\text{year}^{-1}] \;;\; f(T) = \frac{m^{T-T_c}-1}{m^{T_r-T_c}-1} \tag{6.2}$$

in which t [years] is time, k_1 and k_2 are coefficients, $f(T)$ is a correction function for temperature, m is a dimensionless temperature scale, T_c is the lowest temperature at which decomposition of organic matter occurs, T_r is a reference temperature, and T is the actual temperature, t_{age} represents the initial age of the organic matter.

The coefficients k_1 and k_2 are based on a large data set (Middelburg, 1989): k_1 = 0.178, k_2 = -0.95. In Fig.4.5 (section 4.1) a linear temperature effect is found, which can be simulated with $m \approx 1.001$. The reference temperature T_r is 20 ^{o}C and the critical temperature T_r is 6.76 ^{o}C. The 2nd order model is shown in Fig.6.3 and starts in 1884 AD for the wood layer. The decay of organic matter is such that it equals the amount of organic matter and measured decay rate in 2007.

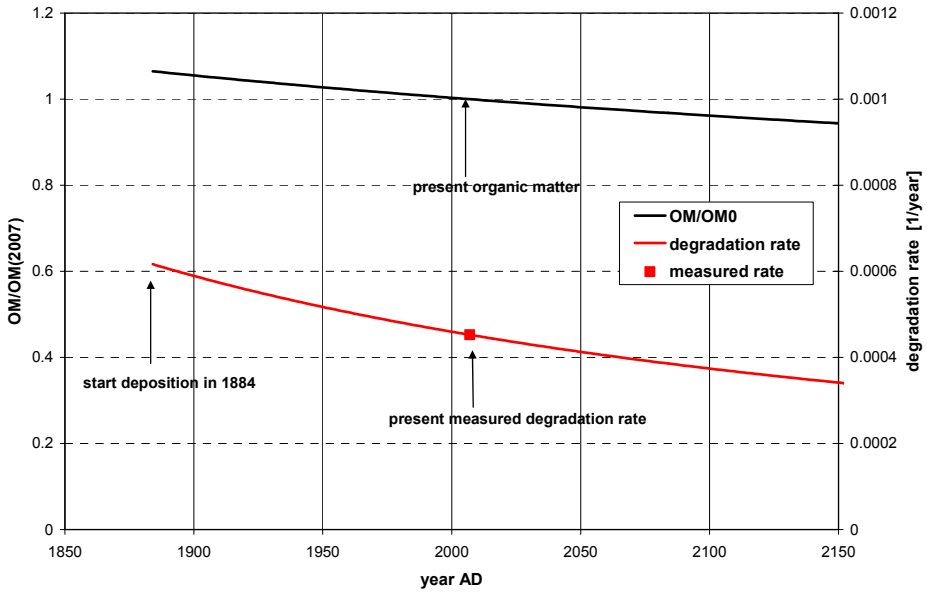

Figure 6.3 Decay of organic matter in time

6.4 Simulation Results Alternative #2

The DELCON simulations with variable cap thicknesses were done for the hydraulic dredging option. It was expected that mechanical dredging with a deposition solid content of 40% (see section 6.1) will result in a surface level that is somewhat lower than deposition of hydraulically dredged slurry. Therefore the mechanical dredging is compared with hydraulic dredging after consolidation including creep.

As indicated with the timeline (Fig.6.1) the DELCON simulations started in 1650 AD. For all boxes 1 to 5 the simulations were done until May 2007, just before deposition of dredged material starts. The dredged in-situ volume is 68,857 cy and will be dredged with a time averaged capacity of 428 cy/day (see section 6.1). With an in-situ averaged solids content of 44.9% and solid density of 1889 kg/m^3 (see Table 5.3) the total dredged solids is 20803 cyds or 15905 m^3 and the solids production rate is 0.001146 m^3/s. The solids deposition flux in the CDF is equal to the solids production rate. However the total discharge into the CDF is determined by dilution during hydraulic dredging. As discussed in section 5.4.5 the solid content of 18% for the hydraulically dredged slurry will result in segregation with relative high settling velocities; the minimum solid content for a non-segregated slurry is 28% or maximum void ratio of 4.867 (see Table 5.3). This yields a total discharge of 0.00672 m^3/s.

It is assumed that the dredged material is pumped in with a sub-aqueous tremie at the deepest area box B5 (see Fig.5.5). The deposition rate is then determined by the surface area of B5. When the top level of the slurry reaches the level of box B4, this area is flooded with the slurry and the deposition rate is than determined by the surface area of B5 and B4. The same procedure is followed until Box 1 is flooded also. The times that each subsequent box is flooded depends on the consolidation that takes place during deposition. After box B1 flooded the simulation is continued until a maximum level is reached. The most shallow area box B1 is reaching that level first. For the remaining boxes the deposition rate will increase, because the area of box B1 is not available anymore. During this last stage of filling the boxes B2 through B5 are subsequently filled up to the maximum level and with increasing deposition rate. The times of flooding, reaching the maximum and deposition rates in meter solids per second are listed in Table 6.1. The above sequence of filling the CDF means in practice that the decanting box for the effluent should be located at the deepest point near the sheet pile wall.

In order to determine the maximum level that can store the total dredged solids of 20803 cyds (15905 m^3), three maximum levels were applied resulting in three total dredged solids volumes (see Fig.6.4): starting with 602 ft, than 604 ft and in between 603.6 ft. By interpolation the final level of 603.69 ft was obtained, which has been used for the final computations.

Table 6.1 Times and deposition rates used in DELCON, alternative #2

box	time flooded [days]	time max level [days]	deposition rate solids [m/s]
#1	73.75	147.57	3.921E-08
#2	30.04	154.06	4.924E-08
#3	12.70	157.67	6.964E-08
#4	4.72	159.69	9.915E-08
#5	0.00	160.51	1.955E-07

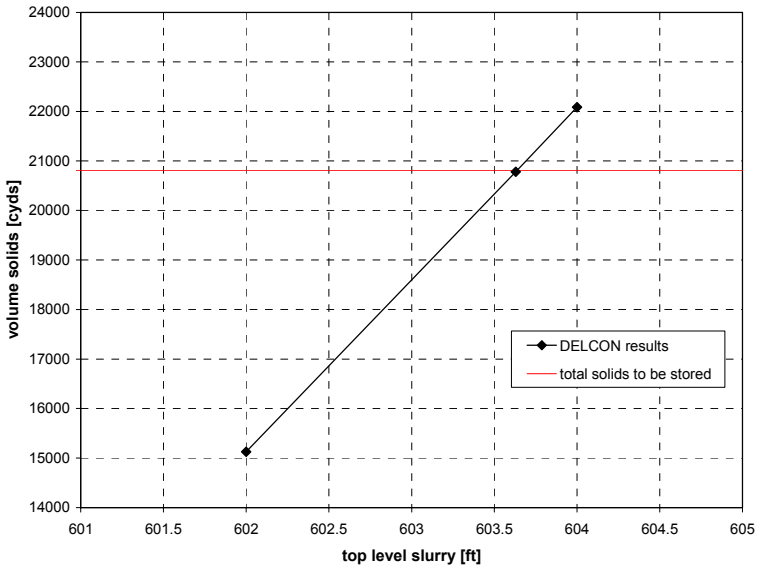

Figure 6.4 Determination of maximum deposition level in CDF

For capping with sand the same dredging capacity of 428 cy/day is assumed. The practical density range for hydraulic sand transport is about 1200 kg/m^3 to maximum 1600 kg/m^3. For the deposition rate a density of 1400 kg/m^3 was used. This yields an averaged solids deposition flux of 0.003097 m^3/s. With a total surface area of 29255 m^2 or 314575 ft^2 a deposition rate of 1.0596E-07 m/s results for all boxes and all cap layer thicknesses.

Typical results of the DELCON simulations are shown in Fig.6.5a through Fig.6.5d in which for box B4 profiles of void ratio, excess pore water pressure, discharge of pore water and methane concentrations are shown for different times: just before capping, during capping (after 20 days) and when capping is finished. The results are shown for 2 ft cap.

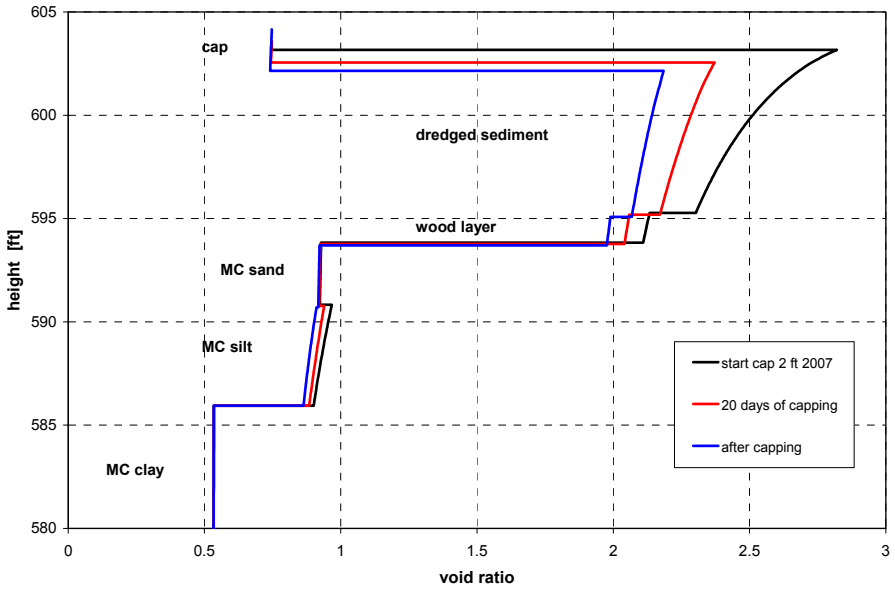

Figure 6.5a Profiles void ratio in box B4

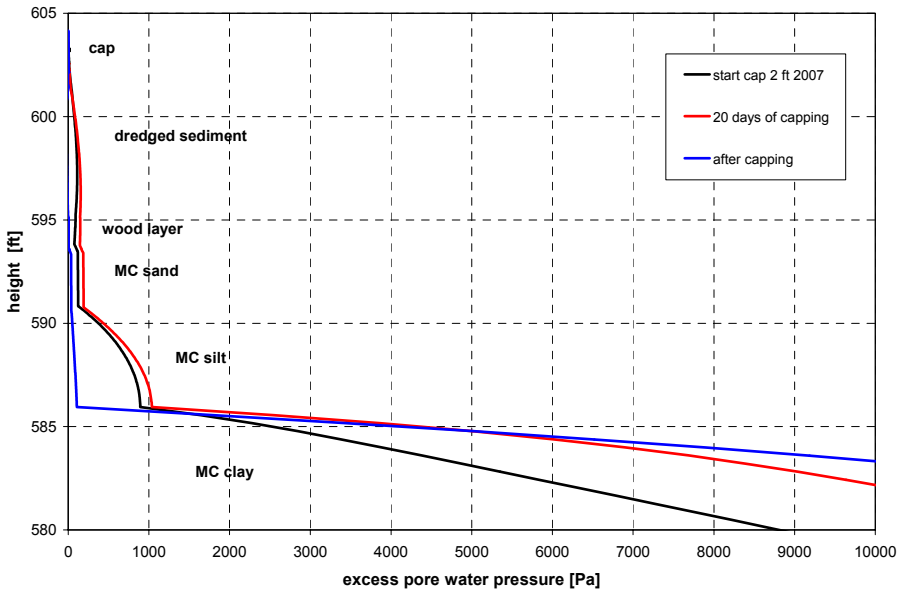

Figure 6.5b Profiles excess pore water pressure in box B4

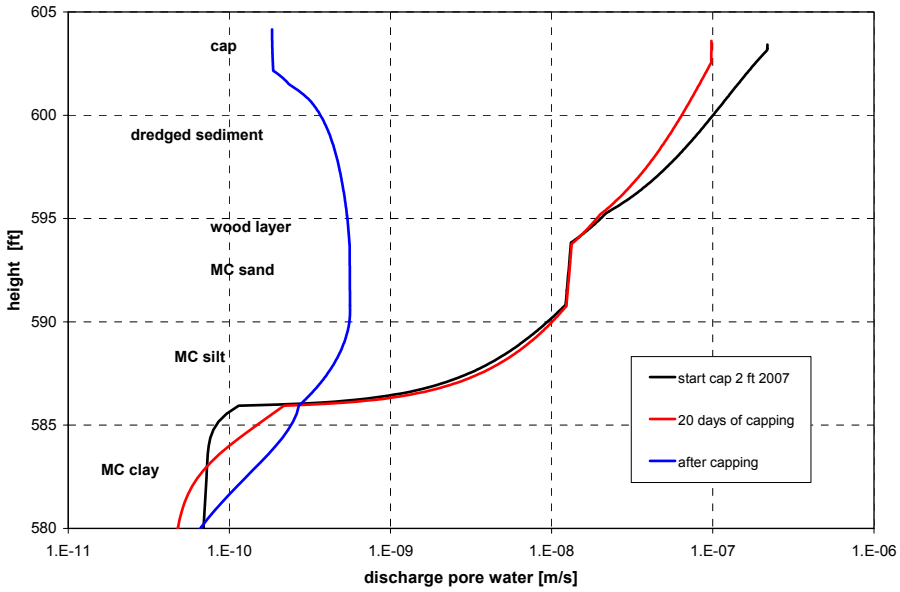

Figure 6.5c Profiles specific discharge in box B4

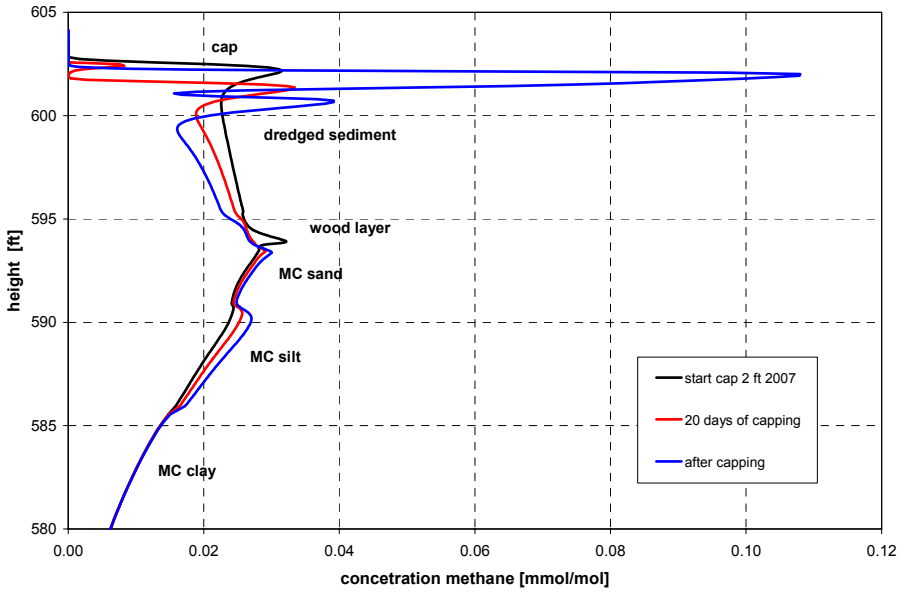

Figure 6.5d Profiles methane concentration in box B4

It can be observed in Fig.6.5b that the generated excess pore water pressures in the wood layer and deposited dredged sediment consolidate very rapidly and actually can follow the deposition and capping. This can be explained by the time scale of consolidation. Eq.(3.5) and a layer thickness of wood layer plus dredged sediment of maximal 10 ft (3 m) with only drainage on top, yields a time scale of 17 days, which is much shorter than the time of slurry depositing and capping. After capping only excess pore pressure remain in the Miller Creek clay for a period of 5 years (see section 5.4.1). The drop in discharge after capping in Fig.6.5c also shows the rapid

consolidation of the wood layer and dredged sediment. Given the rapid consolidation during deposition there will be no advantage to splitting up the deposition of the dredged material into two years.

The methane concentration in Fig.6.5d shows an increase in peak concentration during capping. Although capping insulates the sediment and should reduce methane concentrations, the capping is done during summertime and therefore gas production, which is temperature dependent, will be maximal.

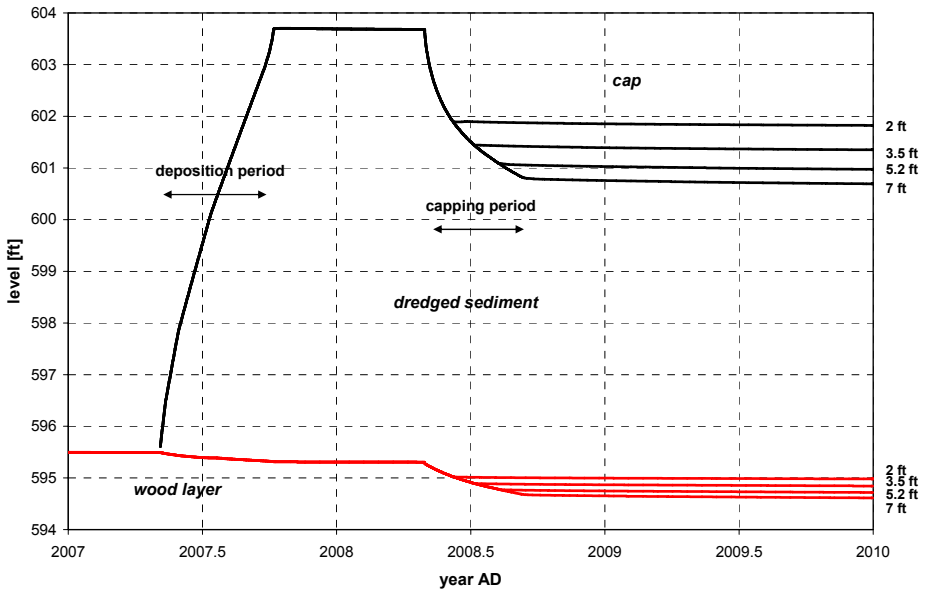

Figure 6.6a Time series levels of wood layer and dredged sediment (B4)

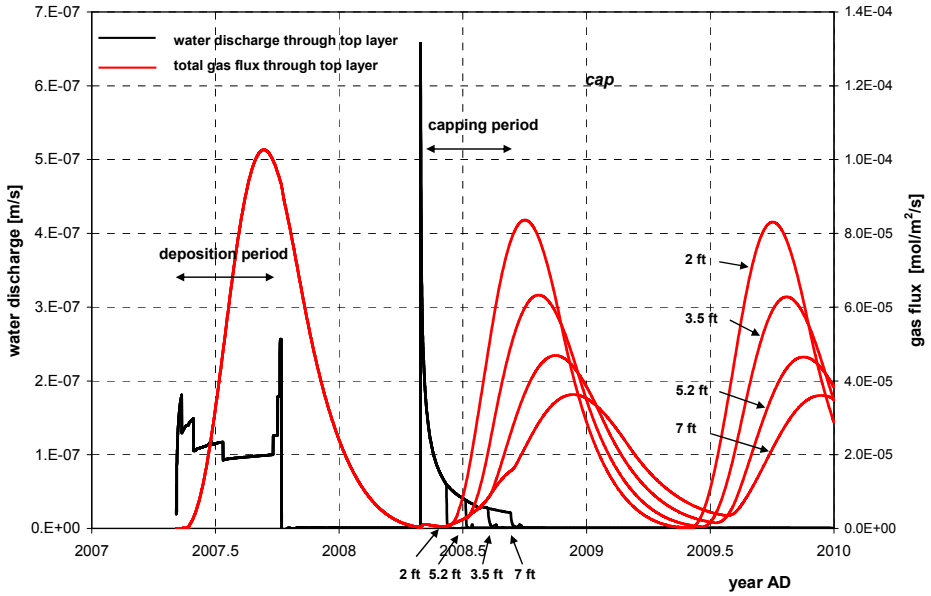

Figure 6.6b Time series water discharge and gas flux through top dredged sediment (B4)

In Fig.6.6a and Fig.6.6b time series are given for top level of layers, specific water discharge, gas flux through lake bed and through top of deposited slurry. In Fig.6.6a the rapid consolidation during deposition and capping can be observed as well. The settling after capping is creep of the wood layer and deposited slurry.

The water discharge through the top of the slurry layer (black lines in Fig.6.6b) is maximal at the start of capping. Because the deposition rate for all cap layer thicknesses is the same the discharge is independent of cap layer thickness. In Table 6.2 the maximum values are given together with the surface areas and total discharge. These discharges are much smaller than the discharge necessary to mobilize NAPL: 0.75 m/day (see section 3.3.2). Therefore no NAPL displacement is expected, but NAPL will be redistributed in the pore system.

The gas flux through the top of the sediment layer (red lines in Fig.6.6b) is affected by the cap layer thickness due to the heat insulating effect. A thicker cap results in less gas release.

Table 6.2 Maximum water discharges during capping

box	surface area [ft^2]	specific discharge [m/day]	discharge [m^3/hr]
#1	64098	0.0446	11.07
#2	73379	0.0516	14.66
#3	52716	0.0522	10.65
#4	61291	0.0568	13.48
#5	63091	0.0583	14.24
sum	314575		64.09

In Fig.6.7 the time series and profile results are combined in a colored plot with contours for void ratio (Fig.6.7a), temperature in ^oC (Fig.6.7b) and methane concentration in mmol/mol (Fig.6.7c). These figures are given for box B4 with a 2 ft cap and have the same time frame as Fig.6.6: 2007 until 2010. The void ratio plot (Fig.6.7a) shows a rapid consolidation during deposition. After the sand cap is deposited the void ratio is still changes in time due to creep. Note that the top level of the cap is almost the same as the level of the dredged sediment before capping. In Fig.6.7b the temperature variation with depth and time is given. After capping it shows that the temperatures in the dredged sediment are reduced due to the insulating effect of the cap. In Fig.6.7c the methane concentration is depicted. The highest concentrations occur in areas with highest temperatures (Fig.6.7b). During the placement of the sand cap very low concentrations appear (brown area) in the dredged sediment. This is a result of the increased upward advective transport due to local consolidation. After the cap is placed diffusive transport into the cap layer can be observed. In case of a membrane in between the sand cap and top of dredged sediment (see Fig.6.2) gas will be trapped below the membrane.

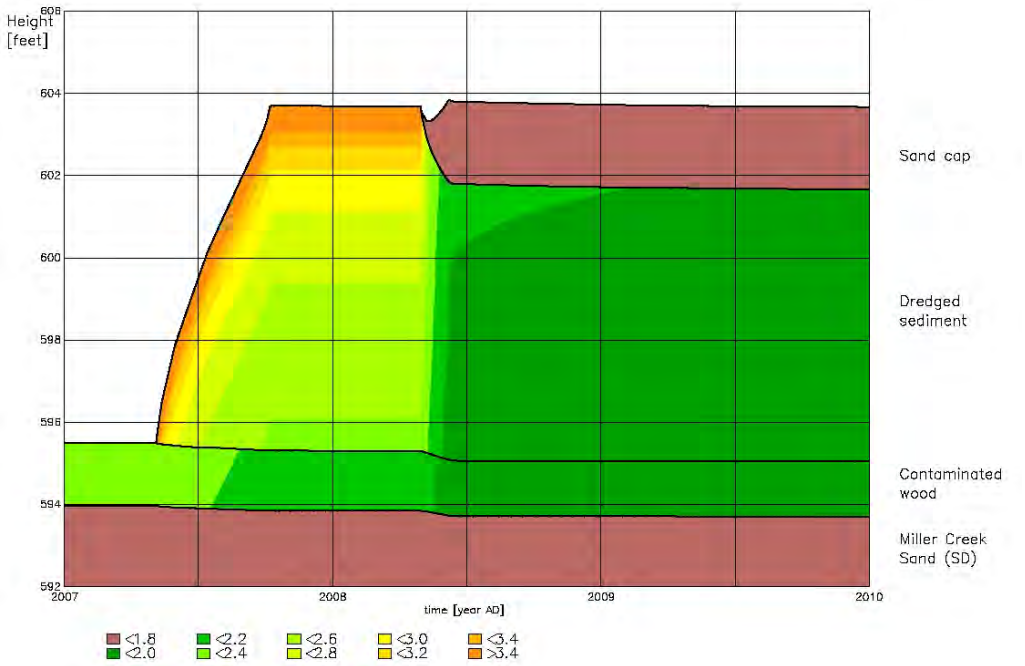

Figure 6.7a Void ratio as function of time and depth in box B4

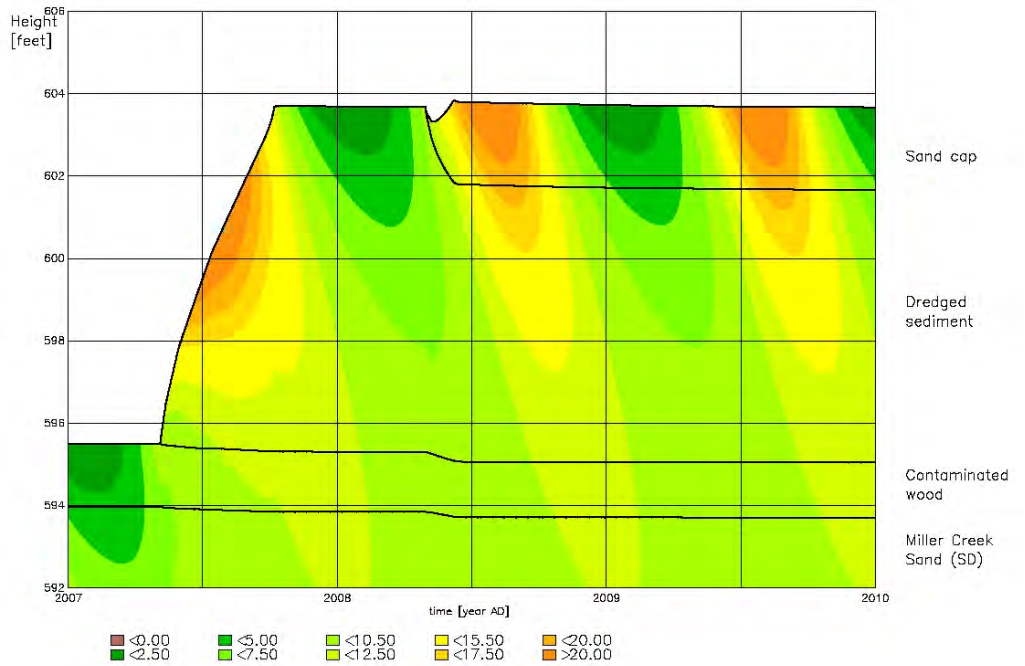

Figure 6.7b Temperature in ^{o}C as function of time and depth in box B4

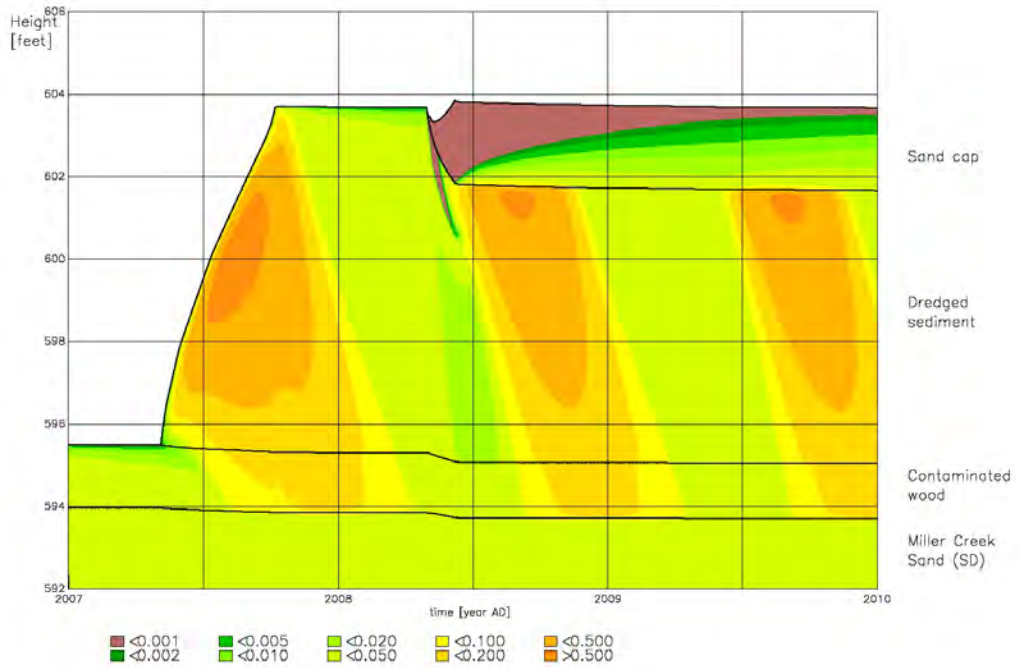

Figure 6.7c Methane concentrations in mmol/mol as function of time and depth in box B4

In Fig.6.8 the settling of layers are shown for all 5 boxes, by plotting the settlements as function of the cumulative surface area. Depicted are the top of Miller Creek sand, contaminated wood layer, dredged sediment deposit and cap layer (3.5 ft) for 4 times: just before deposition of dredged sediment (2007), after deposition (2008), after capping (2010) and long term settlement (2100). The settlement in box B4 and B5 are maximal. This is caused by the combination of large amount of dredged sediment and a thick wood layer. Near the sheet pile (box B5) settlement is somewhat less, because the wood layer is very thin and deposition was continuing until the end, while the other boxes stopped earlier (see Table 6.1). Near the shoreline (box B1) the final level is maximal due to the shallow height of the dredged material. The final top level of the dredged sediment (2100 AD) in each box is listed in Table 6.3 for all 4 cap layer thicknesses. In Table 6.4 the settlements are given for the top of the dredged sediment in each box and for all cap layer thickness. The averaged final height (in 2100 AD) is depicted in Fig.6.9 together with the averaged level of the top of dredged sediment. From this graph it can be concluded that a cap of 1.5 ft is sufficient to get the averaged top level of the dredged sediment below 602 ft. Further increase of the cap layer thickness gives less settlement. In Fig.6.9 also the final top levels are shown for mechanical dredging. It is assumed that mechanical dredging does not dilute the dredged sediment. The effect however on the final level in 2100 is less than 0.18 ft with respect to hydraulic dredging assuming no segregation, which can be achieved at a solid content above 28%.

In the event the solid content of the dredge material is less than 28%, segregation of the coarse fraction (mainly sand 63% by weight) will result in less consolidation of the fines and wood fibers in the CDF. Under these conditions the sand fraction

builds its own “skeleton”, i.e. sand particles rest on other sand particles, and as a result the full weight of the particulate portion of the dredge slurry is not effectively consolidating the fines and wood fibers. This will result in a much higher final layer thickness of the dredge material, perhaps by a factor of 2.

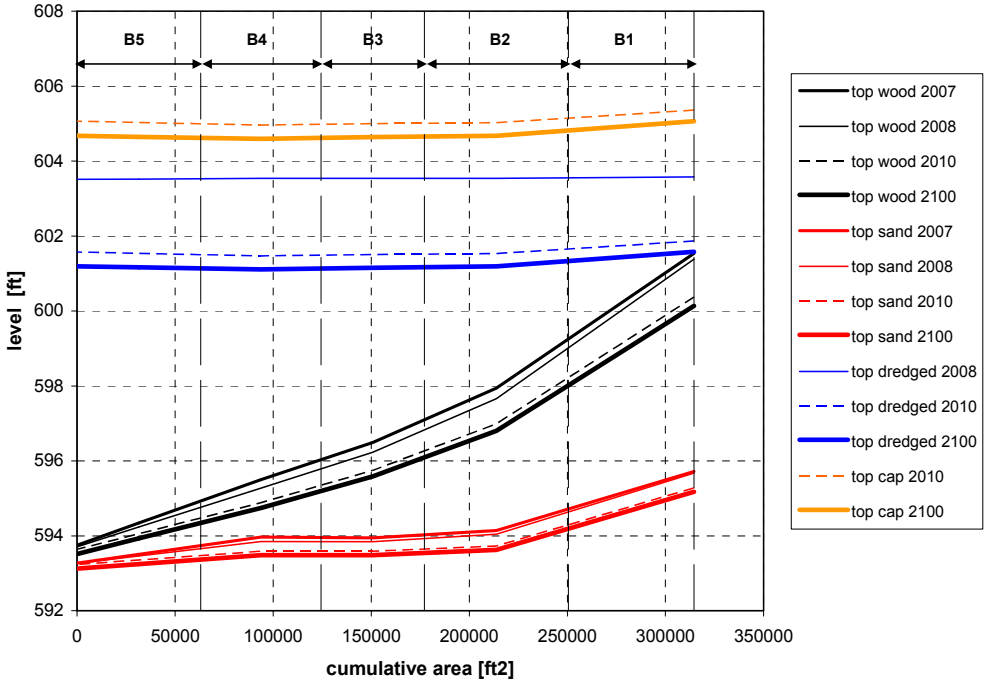

Figure 6.8 Settling profiles cap 3.5 ft

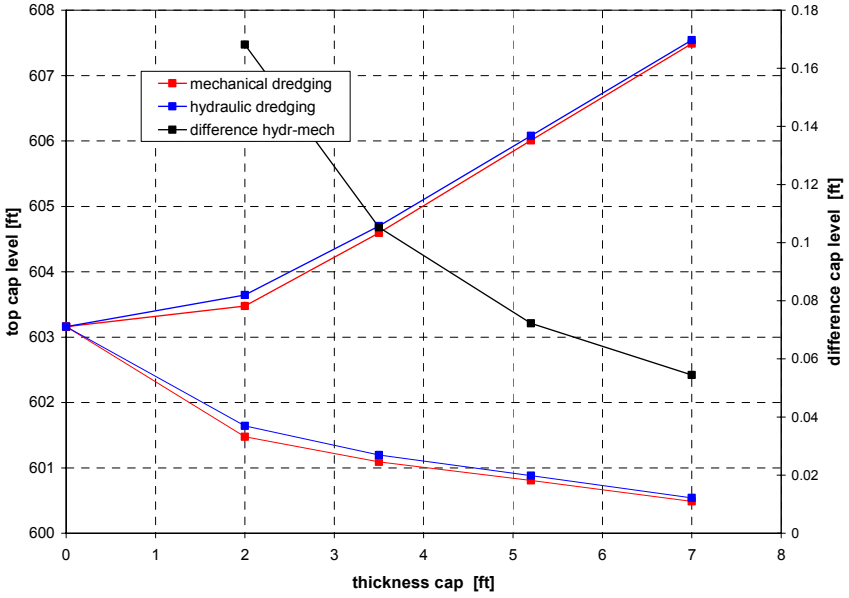

Figure 6.9 Averaged top level of dredged sediment and cap for hydraulic and mechanical dredging

Table 6.3 Final top level dredged sediment in 2100 AD

cap thickness [ft]	B 1 [ft]	B 2 [ft]	B3 [ft]	B4 [ft]	B5 [ft]
2	601.87	601.63	601.59	601.55	601.57
3.5	601.45	601.19	601.15	601.11	601.16
5.2	601.10	600.82	600.79	600.75	600.83
7	600.83	600.55	600.52	600.48	600.58

Table 6.4 Final settlement top level dredged sediment in 2100 AD

cap thickness [ft]	B 1 [ft]	B 2 [ft]	B3 [ft]	B4 [ft]	B5 [ft]
2	-1.69	-1.91	-1.95	-1.99	-1.95
3.5	-2.11	-2.35	-2.39	-2.43	-2.36
5.2	-2.46	-2.72	-2.74	-2.79	-2.69
7	-2.73	-3.00	-3.01	-3.06	-2.94

6.5 Simulation Results - Alternative #3

Alternative #3 (see section 6.1) considers two dredging depths: 4ft (#3a) and 2 ft (#3b). In order to determine the final height of the lakebed, different cap layer thicknesses were simulated with DELCON in each box. Given the layer thickness of the wood layer in each box as depicted in Fig.5.5, a 4 ft dredging depth will remove the whole contaminated wood layer in box B2, B3, B4 and B5. In case of 3 ft dredge depth only in box B3, B4 and B5 the wood layer is completely removed. For a 2 ft dredging depth this holds only for box B4 and B5. The DELCON simulations were done for the boxes where a compressible wood layer is still present. In the other boxes, the compressibility of the remaining soil layers are very low which will always result in a higher seabed level. In Table 6.5 the computed cap layer thickness are given that result in the same seabed level. Also in this alternative the discharges of pore water during capping are below the threshold for NAPL movement.

Table 6.5 Cap layer thickness for constant sea bed level

dredging depth [ft]	B 1 [ft]	B 2 [ft]	B3 [ft]	B4 [ft]	B5 [ft]
2	2.34	2.32	2.17		
3	3.22	3.32			
4	4.29				

7. Conclusions and Recommendations

7.1 Conclusions

The permeability of the wood layer according to the SIC test show that a solids content less than 28% will be in the hindered settling regime. In the hindered settling regime there is no contact beween particles, but the settling velocity of each fraction is reduced by the volume concentration of solids. In this regime, segregation of fraction can occur during deposition in the CDF. In general, segregation yields a larger volume in the CDF after consolidation with the same total amount of solids. Therefore the DELCON simulations for hydraulically dredged contaminated wood layer were performed at a solid content above 28%.

In the event the solid content of the dredge material is less than 28%, segregation of the coarse fraction (mainly sand 63% by weight) will result in less consolidation of the fines and wood fibers in the CDF. The final layer thickness of the dredge material could be greater by up to a factor of 2 compared to consolidation of dredge material with a solid content greater than 28%.

The permeability of the contaminated wood layer under the CDF and the dredged contaminated sediment is such that consolidation times are less than 17 days, which is much less than the slurry deposition time and capping time of maximum 180 days. The drainage of these layers is almost instantaneously when loaded in a rate that corresponds to the capacity of the dredging equipment (428 cyds/day). The remaining settlement is mainly due to creep of the wood layer and dredged contaminated sediment in the CDF. There will also be some contribution to consolidation by the Miller Creek clay layer, but that will end after the time scale of about 5 years.

Given the rapid consolidation there will be no advantage to phasing deposition of the dredged sediment over two years.

The compressibility of the wood layer is mainly determined by the organic fibers and much less by the mineral fraction, which is mainly silt and sand. The clay fraction is only 3.4% of the mineral fraction and is only able to reduce permeability.

For bubble formation in the wood layer sediment, the air entry value of the wood layer is important. With the measured air entry value of 2.69 kPa the strength of the sediment must be smaller than 360 Pa in order to get bubble formation. A larger strength will result in de-saturation of the pore system. The in-situ strength is about 200 Pa. After consolidation this strength increases above 360 Pa and therefore it is expected that production of methane and carbon dioxide will de-saturate the largest pores and create pathways for gas releases.

The specific discharges through the top layer of the dredged sediment in the CDF during capping with sand are much smaller than the discharge necessary to mobilize NAPL (0.75 m/day). Therefore no NAPL displacement is expected. That holds also for alternative #3.

In order to store the total amount of dredged solids (20,803 cyds) in the CDF, the level of the hydraulically dredged slurry must be maximum 603.64 ft. A cap thickness of 1.5 ft is sufficient to get the averaged top level of the dredged sediment below 602 ft.

The effect of mechanical dredging is almost the same as hydraulic dredging, due to the rapid consolidation of the wood layer material. Mechanical dredging will result in a lower final level than with hydraulic dredging, however the difference in final level is less than 0.18 ft.

The required cap layer thickness in Alternative #3 to get the same lake bed level after capping is slightly more than the dredging depth.

7.2 Recommendations

The permeability of the wood layer according to the SIC test show that a solids content of 28% or lower will be in the hindered settling regime and therefore result in a lot of segregation in pipeline transport and deposition in the CDF. It is recommended to perform settling test at different diluted concentration in order to determine segregation levels.

If hydraulic dredging is anticipated and it appears that the solids content of he dredge material will be less than 28%, then these conditions should be modeled as part of remedial design.

Given the sequence of filling in the CDF, where the deepest point in the CDF gets the last solids at the end of filling, it is recommended to locate the decanting box for the effluent at the deepest point near the sheet pile wall.

In the present study no information was available about the volume concentration and size characteristics of the large logs present in the contaminated wood layer. The structure of these logs is unknown and could hamper consolidation of the existing wood layer. The percent of large logs by volume will reduce settlement by at least 10%, but could be more if the sediment in between the logs remains under-consolidated.

8. References

Marle, C.M. 1981 Multiphase flow in porous media, Gulf Publishing Company Houston Texas.

URS. 2007. Remedial Investigation Report. Ashland/Northern States Power Lakefront Superfund Site.

Winterwerp, J.C. and W.G.M. van Kesteren. 2004. Introduction to the Physics of Cohesive Sediment in the Marine Environment, in Development in Sedimentology 56, Elsevier.

Appendix A

Soil Engineering Testing

CONSOLIDATION TEST REPORT

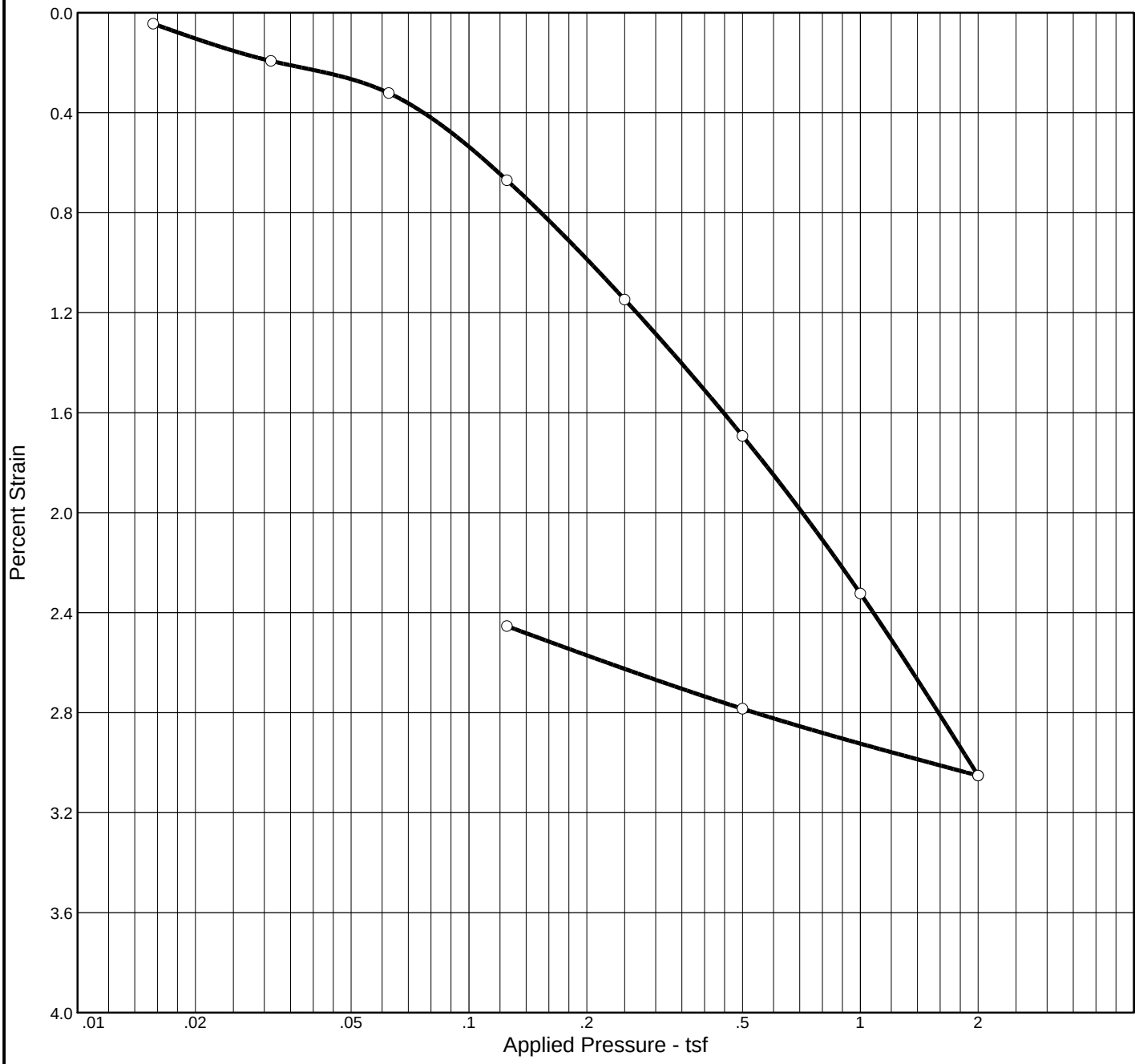

Natural		Dry Dens. (pcf)	LL	PI	Sp. Gr.	Overburden (tsf)	P_c (tsf)	C_c	C_r	Swell Press. (tsf)	Swell %	e_o
Sat.	Moist.											
100.0 %	29.3 %	96.4	----	----	2.82	0.13	0.18	0.04	0.01			0.827

MATERIAL DESCRIPTION	USCS	AASHTO
Medium dense,wet,tan, silty fine Sand SM	SM	----

Project No. 07-2183 **Client:** URS Corp.

Project: Ashland Superfund, WI.
Project No. 25688375

Location: Flux Column 2G Sediment at Bottom

SOIL TECHNOLOGY

Bainbridge Island, WA

Remarks:

Bottom 1- 3 cm sediment after flux w/ 2.9 ft. sand cap

Figure 1

Dial Reading vs. Time

Project No.: 07-2183
Project: Ashland Superfund, WI.
Project No. 25688375
Location: Flux Column 2G Sediment at Bottom

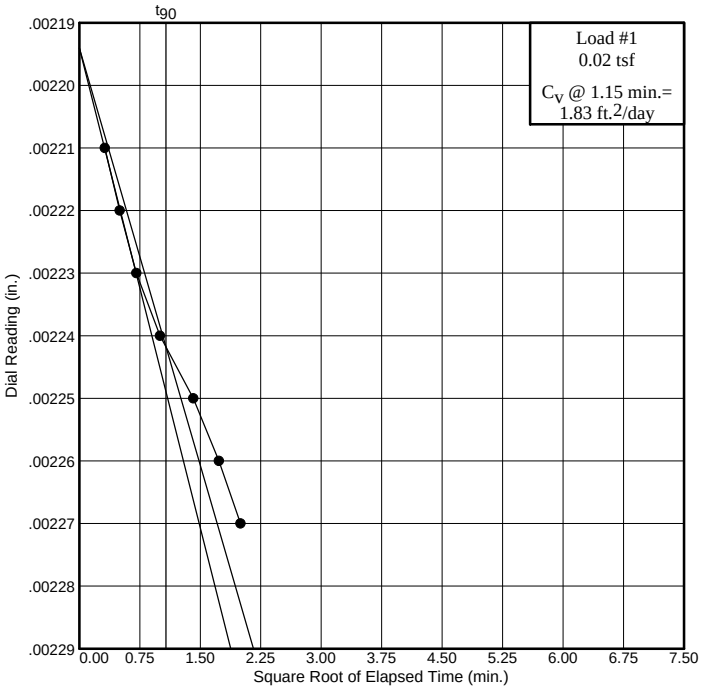

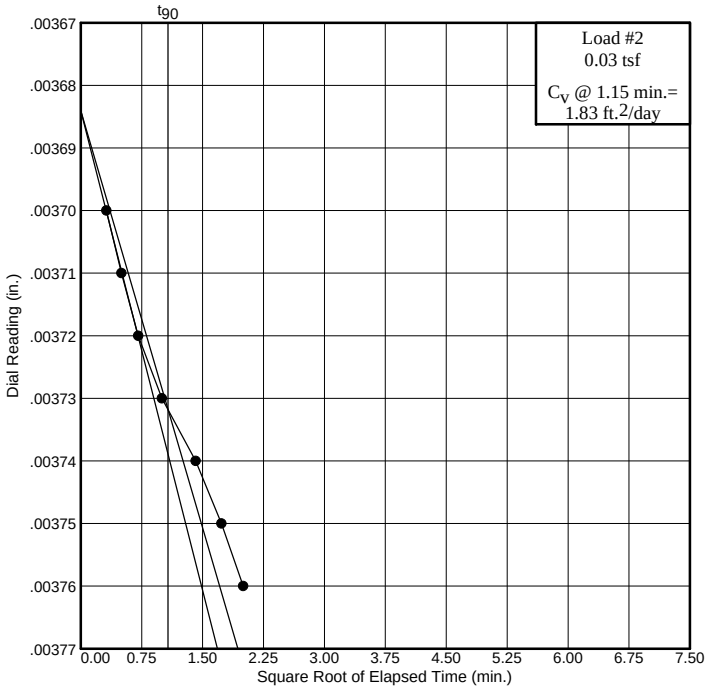

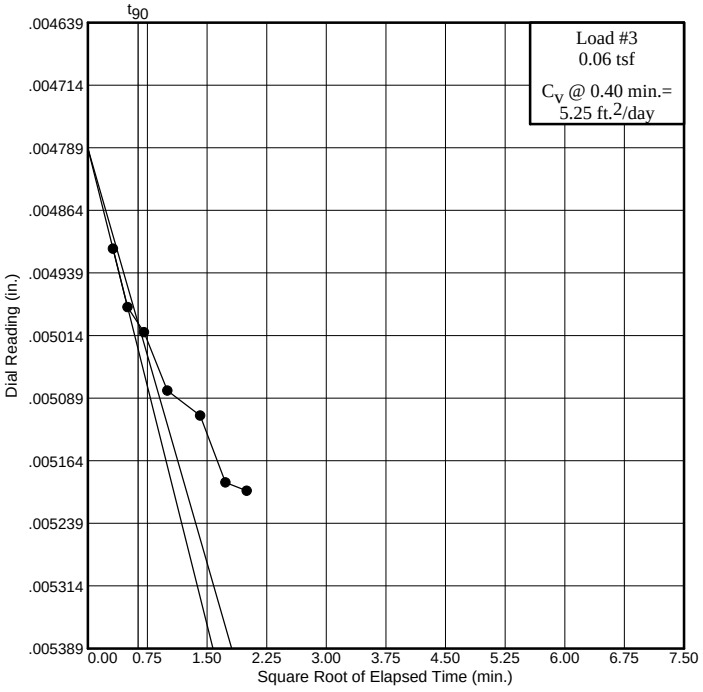

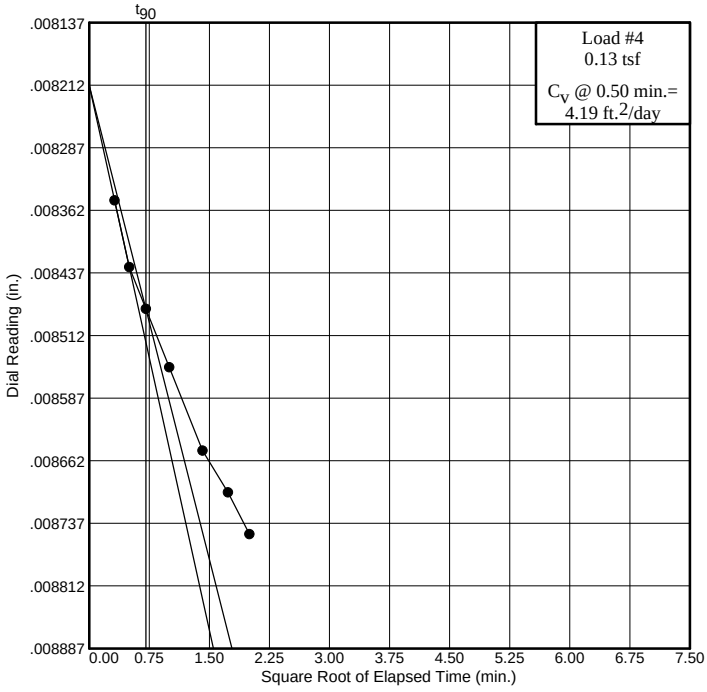

SOIL TECHNOLOGY

Bainbridge Island, WA

Figure 2

Dial Reading vs. Time

Project No.: 07-2183
Project: Ashland Superfund, WI.
Project No. 25688375
Location: Flux Column 2G Sediment at Bottom

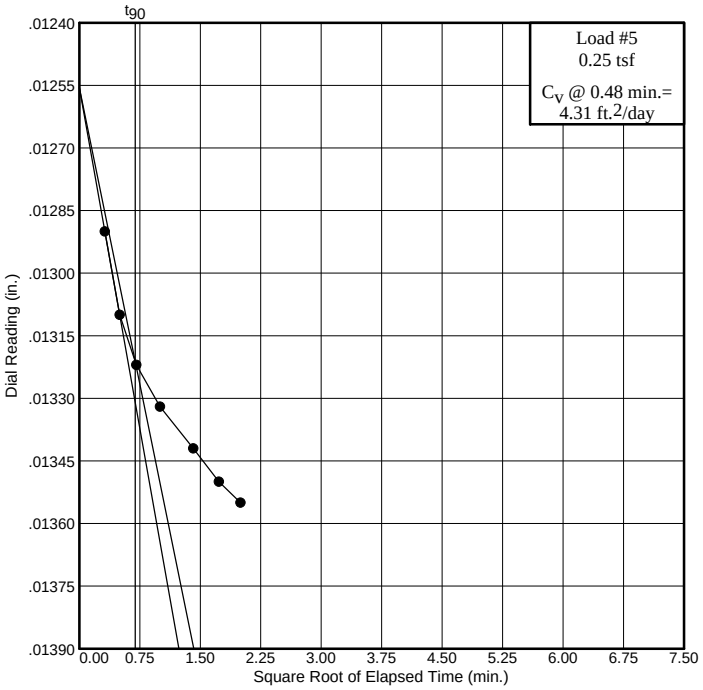

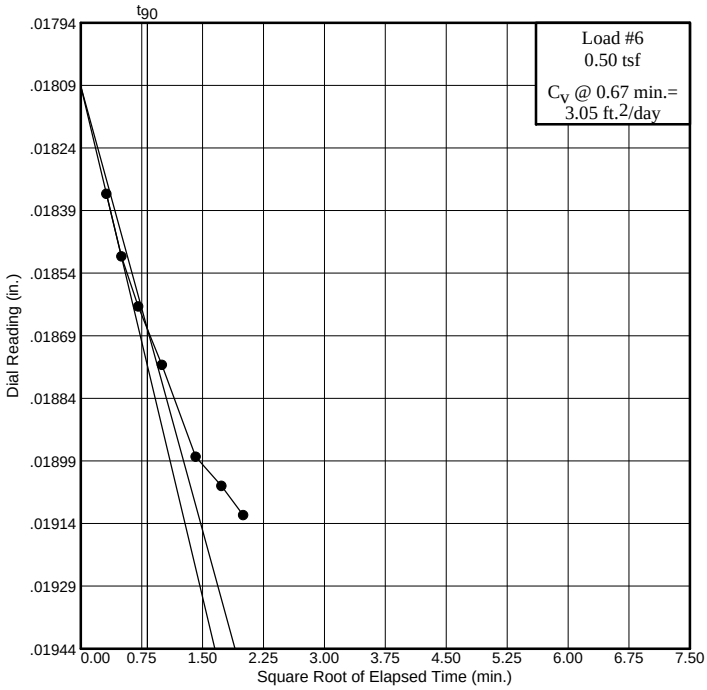

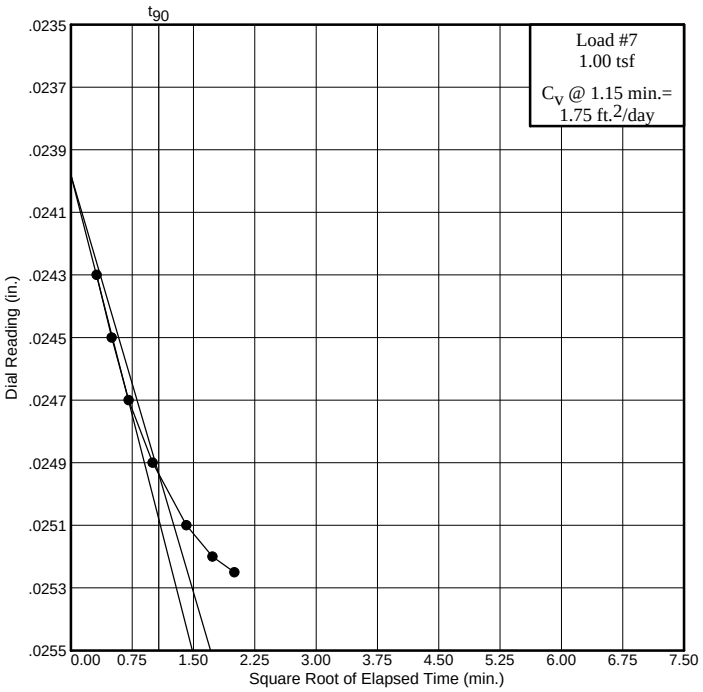

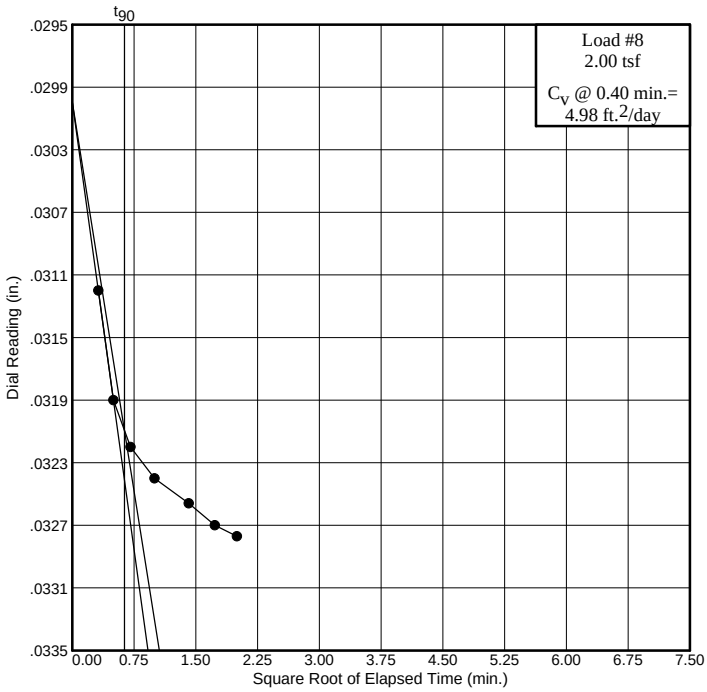

SOIL TECHNOLOGY

Bainbridge Island, WA

Figure 3

Dial Reading vs. Time

Project No.: 07-2183
Project: Ashland Superfund, WI.
Project No. 25688375
Location: Flux Column 2G Sediment at Bottom

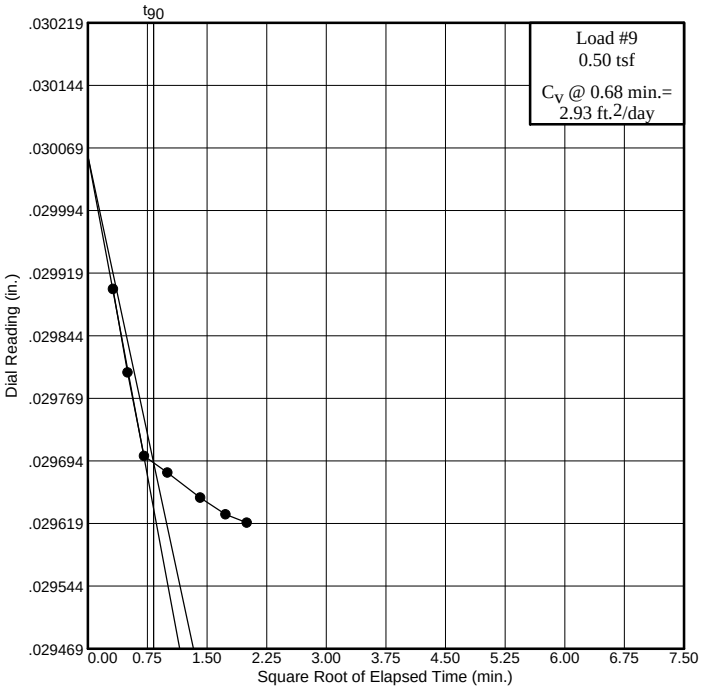

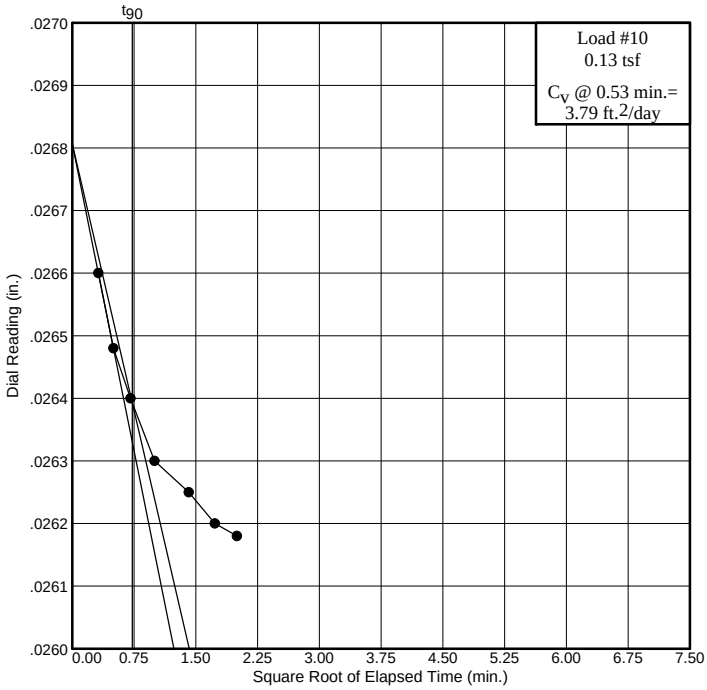

SOIL TECHNOLOGY

Bainbridge Island, WA

Figure 4

CONSOLIDATION TEST REPORT

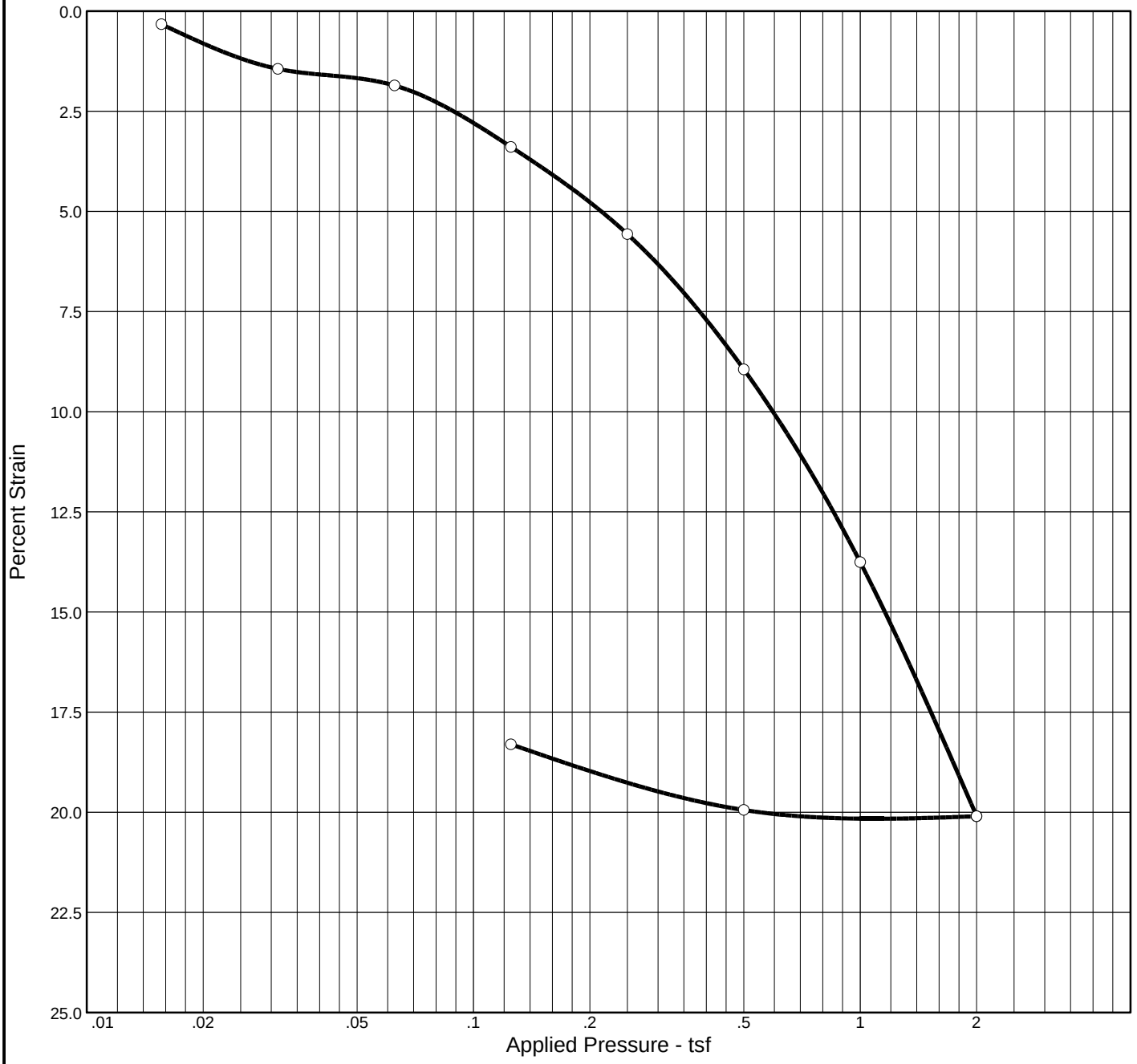

Natural		Dry Dens. (pcf)	LL	PI	Sp. Gr.	Overburden (tsf)	P_c (tsf)	C_c	C_r	Swell Press. (tsf)	Swell %	e_o
Sat.	Moist.											
98.8 %	205.3 %	21.9	----	----	1.3	.15 est.	0.46	0.79	0.06			2.700

MATERIAL DESCRIPTION	USCS	AASHTO
Soft to m-stiff,wet,grey-black, wood debris	PT	----

Project No. 07-2183 **Client:** URS Corp.

Project: Ashland Superfund, WI.
Project No. 25688375

Location: Flux Column 2D Wood Debris Layer

SOIL TECHNOLOGY

Bainbridge Island, WA

Remarks:

Wood fiber/debris layer after flux w/ 4.2 ft. sand cap

Figure 2

Dial Reading vs. Time

Project No.: 07-2183
Project: Ashland Superfund, WI.
Project No. 25688375
Location: Flux Column 2D Wood Debris Layer

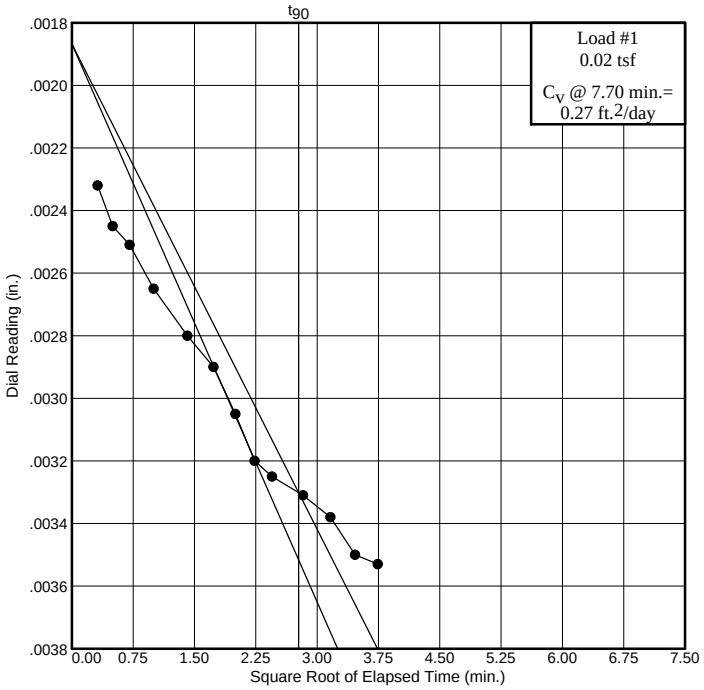

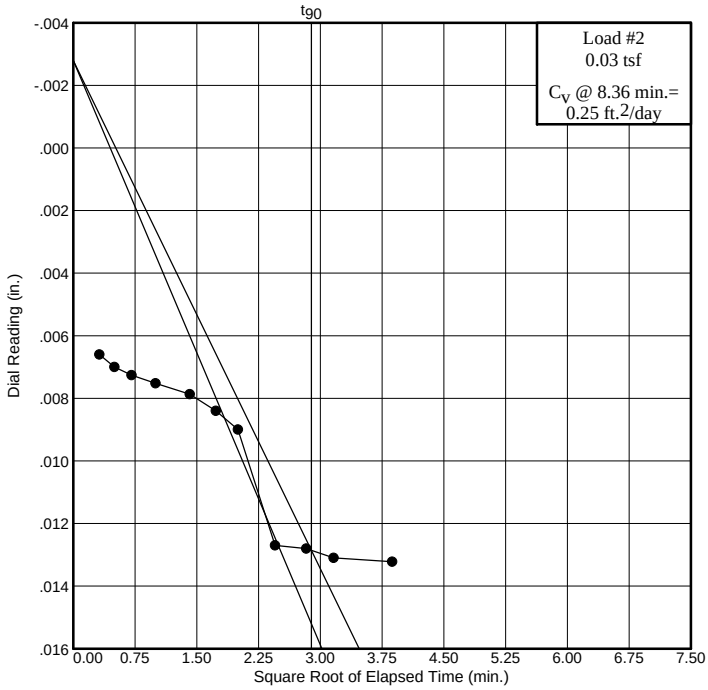

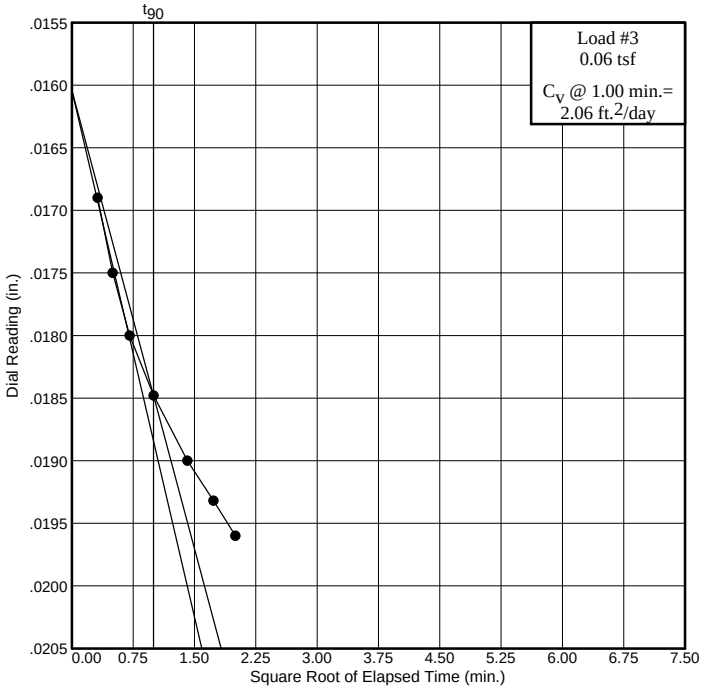

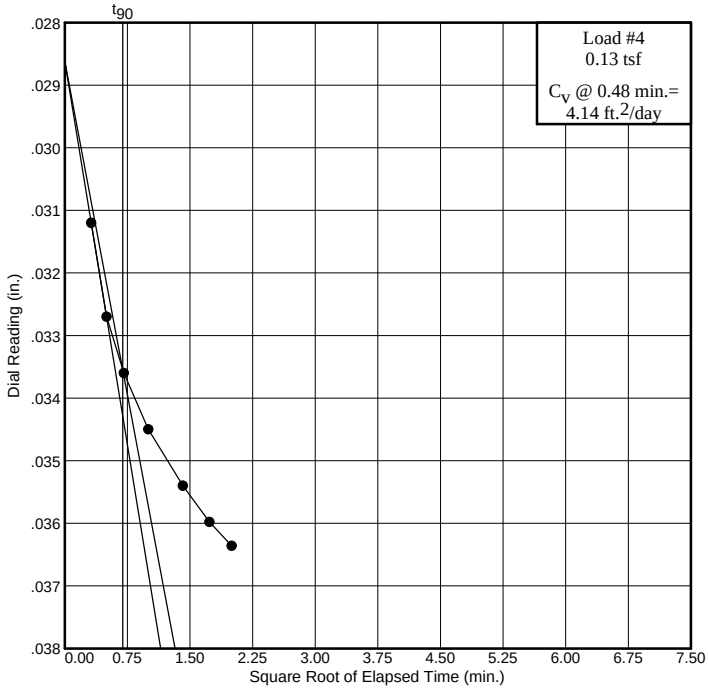

SOIL TECHNOLOGY

Bainbridge Island, WA

Figure 3

Dial Reading vs. Time

Project No.: 07-2183
Project: Ashland Superfund, WI.
Project No. 25688375
Location: Flux Column 2D Wood Debris Layer

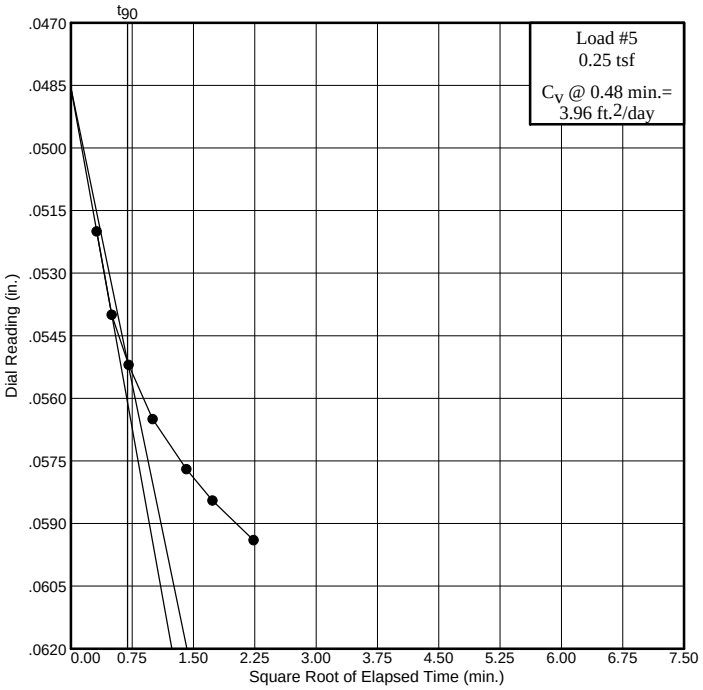

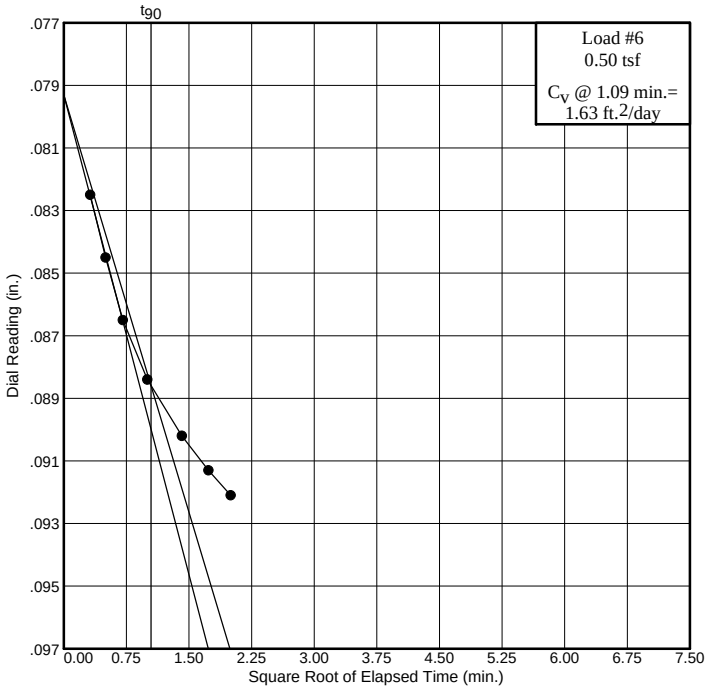

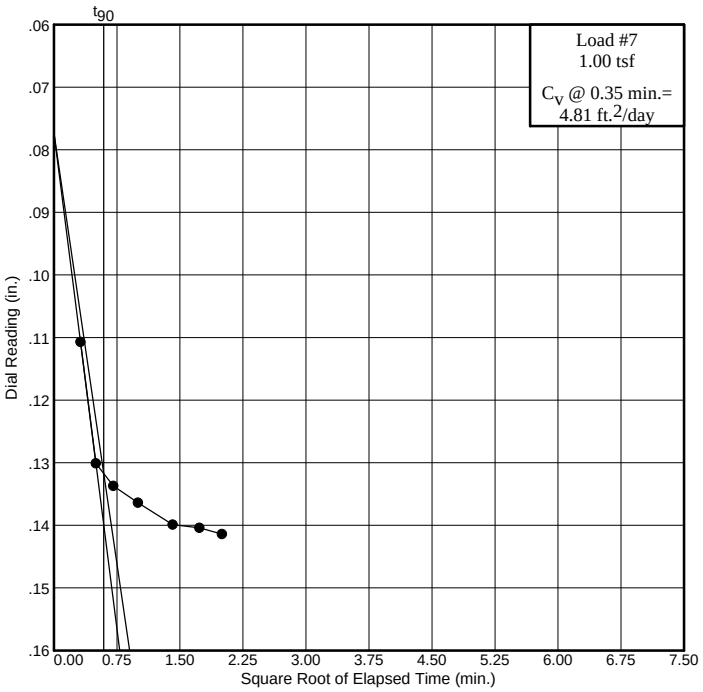

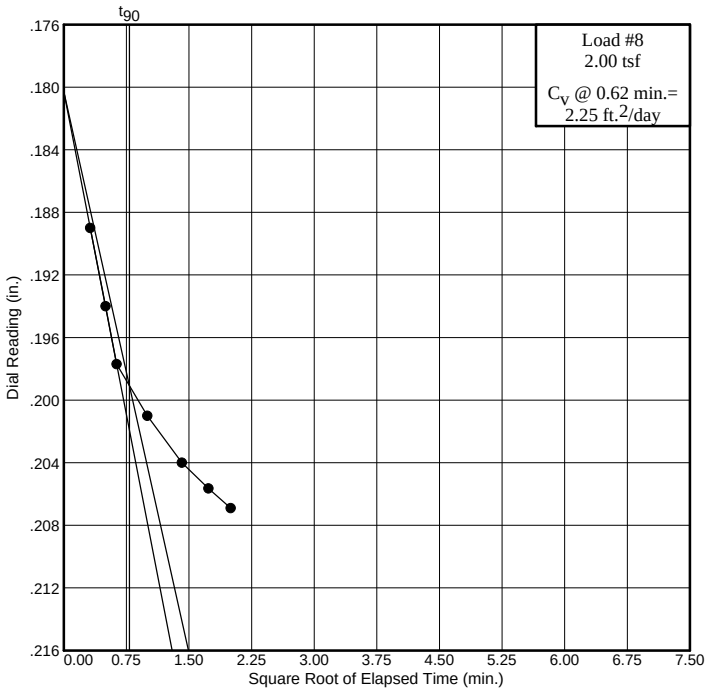

SOIL TECHNOLOGY

Bainbridge Island, WA

Figure 4

Dial Reading vs. Time

Project No.: 07-2183
Project: Ashland Superfund, WI.
Project No. 25688375
Location: Flux Column 2D Wood Debris Layer

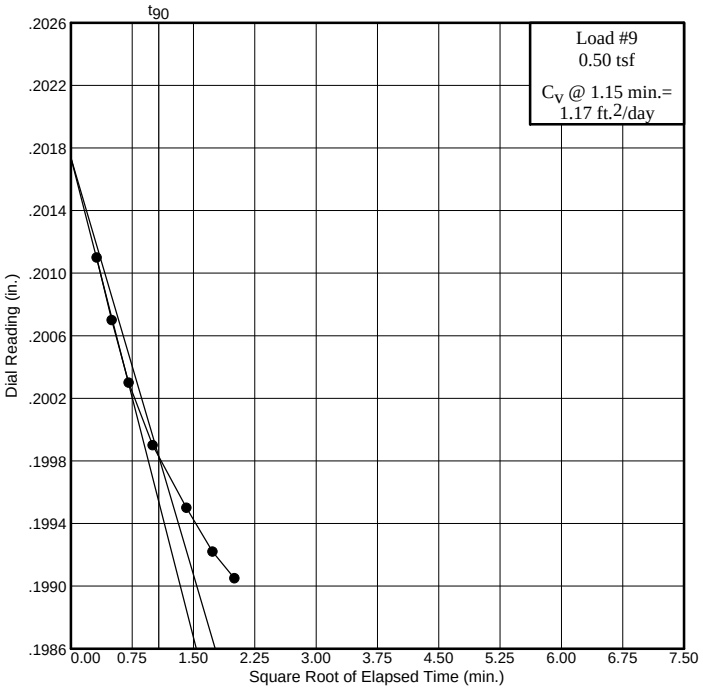

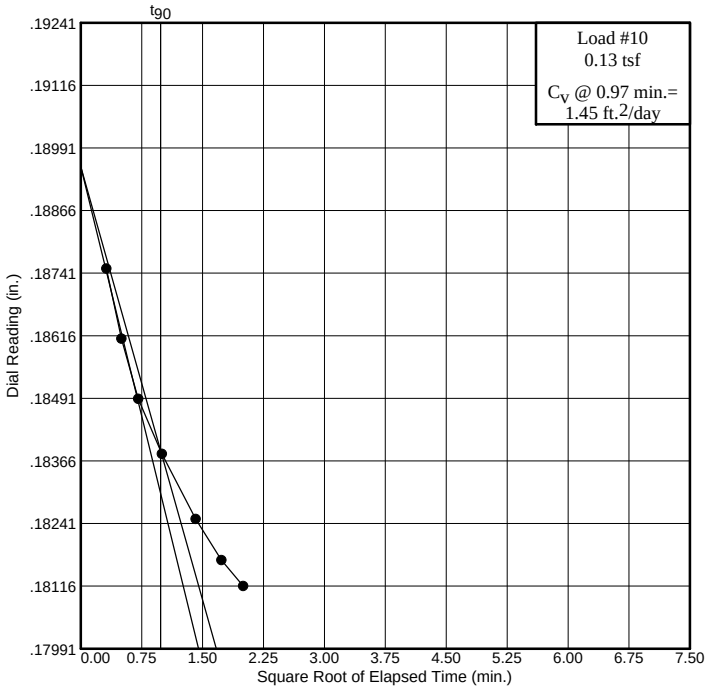

SOIL TECHNOLOGY

Bainbridge Island, WA

Figure 5